AFRL-AFOSR-VA-TR-2021-0030

Long-range Geomagnetic Navigation in Sea Turtles An Interdisciplinary Approach to Localizing Magnetite-based Biological Magnetoreceptors

Lohmann, Kenneth
UNIVERSITY OF NOTH CAROLINA AT CHAPEL HILL
104 AIRPORT DR STE 2200
CHAPEL HILL, NC,
US

04/14/2021
Final Technical Report

Air Force Research Laboratory
Air Force Office of Scientific Research
Arlington, Virginia 22203
Air Force Materiel Command

REPORT DOCUMENTATION PAGE

Form Approved
OMB No. 0704-0188

1. REPORT DATE *(DD-MM-YYYY)*	**2. REPORT TYPE**	**3. DATES COVERED** *(From - To)*
14-04-2021	Final	15 Sep 2014 - 14 Sep 2019

4. TITLE AND SUBTITLE
Long-range Geomagnetic Navigation in Sea Turtles An Interdisciplinary Approach to Localizing Magnetite-based Biological Magnetoreceptors

5a. CONTRACT NUMBER

5b. GRANT NUMBER
FA9550-14-1-0208

5c. PROGRAM ELEMENT NUMBER
61102F

6. AUTHOR(S)
Kenneth Lohmann

5d. PROJECT NUMBER

5e. TASK NUMBER

5f. WORK UNIT NUMBER

7. PERFORMING ORGANIZATION NAME(S) AND ADDRESS(ES)
UNIVERSITY OF NOTH CAROLINA AT CHAPEL HILL
104 AIRPORT DR STE 2200
CHAPEL HILL, NC
US

8. PERFORMING ORGANIZATION REPORT NUMBER

9. SPONSORING/MONITORING AGENCY NAME(S) AND ADDRESS(ES)
AF Office of Scientific Research
875 N. Randolph St. Room 3112
Arlington, VA 22203

10. SPONSOR/MONITOR'S ACRONYM(S)
AFRL/AFOSR RTB2

11. SPONSOR/MONITOR'S REPORT NUMBER(S)
AFRL-AFOSR-VA-TR-2021-0030

12. DISTRIBUTION/AVAILABILITY STATEMENT
A Distribution Unlimited: PB Public Release

13. SUPPLEMENTARY NOTES

14. ABSTRACT

This research involved a three-pronged multidisciplinary approach. In the first, we developed a new magnetomotive optical coherence tomography (MMOCT) system with unprecedented sensitivity. This system can detect small concentrations of magnetic particles in biological tissue and may thus prove useful in the search for magnetite-based magnetoreceptors. The second approach involved identifying candidate genes involved in assembling magnetoreceptors. Specifically, we investigated gene expression after administering a magnetic pulse, a procedure known to disrupt magnetic orientation in several animals and considered to be a diagnostic test for magnetite-based magnetoreception. In trout, 181 genes were differentially expressed after application of a magnetic pulse, including increased expression in six copies of the frim gene, which encodes a subunit of the universal ironbinding and trafficking protein ferritin. In lobsters, a large number of genes (more than 2,500) had differential expression, including many potentially related to iron homeostasis. Results in both animals are consistent with magnetite-based magnetoreception, inasmuch as many of the genes with altered expression might plausibly be linked to repair or replacement of magnetic receptors disrupted by the pulse. Finally, we conducted behavioral and modeling studies including: (1) analyses providing evidence that sea turtles imprint on the magnetic field of their home areas and use this information to navigate back years later; (2) development of a novel behavioral assay for investigating the ability of sea turtles to recognize and learn specific magnetic fields; (3) experiments investigating behavioral effects of pulsed magnetic fields on fish and lobsters; and (4) investigation of strategies and algorithms for magnetic navigation that might be useful in engineered navigation systems.

15. SUBJECT TERMS

16. SECURITY CLASSIFICATION OF:			**17. LIMITATION OF ABSTRACT**	**18. NUMBER OF PAGES**	**19a. NAME OF RESPONSIBLE PERSON**
a. REPORT	**b. ABSTRACT**	**c. THIS PAGE**			PATRICK BRADSHAW
U	U	U	UU	33	**19b. TELEPHONE NUMBER** *(Include area code)* 425-8492

Standard Form 298 (Rev.8/98)
Prescribed by ANSI Std. Z39.18

FINAL REPORT

Long-range Geomagnetic Navigation in Sea Turtles:
An Interdisciplinary Approach to Localizing Magnetite-based Biological Magnetoreceptors

Air Force Office of Scientific Research FA9550-14-1-0208
Funding Opportunity Number BAA-AFOSR-2013-0001
Basic Research Initiative 2: Bio-Sensing of Magnetic Fields

Period of grant, including one-year no-cost extension: 14 September 2014 to 13 September 2020.)

Submitted by:

Kenneth J. Lohmann, Ph.D.
Department of Biology
University of North Carolina at Chapel Hill
Phone: (919) 962-1332
E-mail: KLohmann@email.unc.edu

Amy L. Oldenburg, Ph.D.
Department of Physics and Astronomy
Biomedical Research Imaging Center
University of North Carolina at Chapel Hill
Phone: (919) 962-5003
E-mail: aold@physics.unc.edu

Sönke Johnsen, Ph.D.
Department of Biology
Duke University
Phone: (919) 660-7321
E-mail: SJohnsen@duke.edu

Technical Point of Contact:

Dr. Patrick Bradshaw, AFOSR/RTE
703-588-8492, DSN 425-8492
E-mail: patrick.bradshaw@afosr.af.mil

FINAL REPORT

The objective of this research was to investigate the long-range navigational system of sea turtles and other aquatic animals, with a view toward uncovering the mechanisms that underlie magnetic field detection in animals, as well as obtaining insights into strategies and algorithms of long-distance navigation that can be leveraged for bio-inspired GPS-free navigation systems and other engineering applications. The approach involved a three-pronged interdisciplinary research plan. The first part involved the design and construction of a magnetomotive optical coherence tomography (MMOCT) system with unprecedented sensitivity, so that it could be used to search for magnetite crystals in animals. The second part involved using genomic techniques to determine if aquatic animals possess genes to sequester iron and/or produce magnetite crystals, with a view toward determining where these genes are expressed and where magnetoreceptors are most likely located. The third part involved using behavioral and modeling approaches to study the bio-sensory basis of long-range navigation in animals and to investigate strategies and algorithms of long-distance magnetic navigation.

Research Approach 1: Localization of Magnetite-Based Magnetoreceptors Using MMOCT

Our first research approach involved searching for magnetite-based magnetoreceptors using magnetomotive optical coherence tomography (MMOCT), a new technology that had never been applied to magnetoreception research. Because of its high sensitivity to magnetic particles and high volumetric scan rate, MMOCT provides an unprecedented ability to detect candidate magnetoreceptors in biological tissue.

A major objective of this work was construction of a novel MMOCT system capable of the high tissue volume scan rates needed to detect isolated and rare magnetoreceptors. The novelty of our approach lies in the development of magnetomotive imaging upon a parallel line-field OCT platform, which illuminates the sample with a line-focused beam and enables superior scan rates by merit of the parallelization. A concept diagram and example set of OCT and MMOCT images collected with the novel system are shown in Fig. 1. Because our OCT system

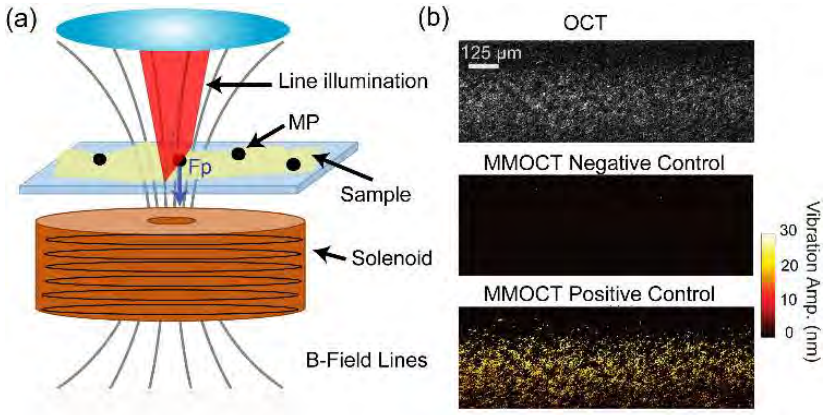

Fig. 1. (a) Schematic diagram of the MMOCT imaging arm configuration with solenoid 5 mm below the sample and the line illumination by a supercontinuum light source above. Magnetic particles (MP) undergo a temporally modulated magnetic gradient force, Fp. (b) Example images (in x-z cross-section) of tissue phantoms including a traditional OCT image (top) showing the light scattering features of the phantom, an MMOCT image from the negative control phantom (middle) and the MMOCT image from the positive control phantom (bottom).

is phase-sensitive, we can sense sub-wavelength (nanometer scale) vibration and bandpass filter motion at the modulation frequency of the magnet to detect magnetically responsive particles. Thus, MMOCT provides *darkfield* contrast to magnetic particles, *i.e.*, the negative control images are dark, which is crucial toward detecting "needle-in-a-haystack" magnetoreceptors.

Below we summarize the major milestones completed during the grant effort, including: (1) development of the novel line-field OCT system (before magnetomotive capability); (2) construction of the magnetic field delivery system for MMOCT; (3) optimization and characterization of the MMOCT system performance; (4) MMOCT imaging of isolated magnetic beads; and (5) initial efforts to image magnetoreceptors in animal tissue samples.

Development of a supercontinuum line-field OCT system

Physics graduate student Jessica Barrick and postdoc Ana Doblas, funded by this project, constructed the system shown in Fig. 2. The parallel OCT system uses a light sheet produced by a cylindrical lens (CL) to illuminate the sample object in a line. Backscattered light is collected in a Michelson interferometer configuration, directed into a grating to spectrally disperse each wavelength component, and captured by a 1024 x 1024 pixel CMOS camera (Photron Fastcam). The parallelization comes from the fact that each transverse position on the sample is encoded as a transverse position on the camera, while the other axis of the camera encodes the wavelength. Using the principles of spectral-domain OCT, a Fourier transform along the wavelength dimension provides the depth-dependent light scattering from the sample object. In contrast to spot-scanning OCT systems which require a camera exposure for each axial line (A-line), parallel OCT requires only one camera exposure to reconstruct an entire 2D frame. With this new system, our frame rate is 1 kHz, a drastic improvement over our flying-spot OCT system operated at 150 Hz.

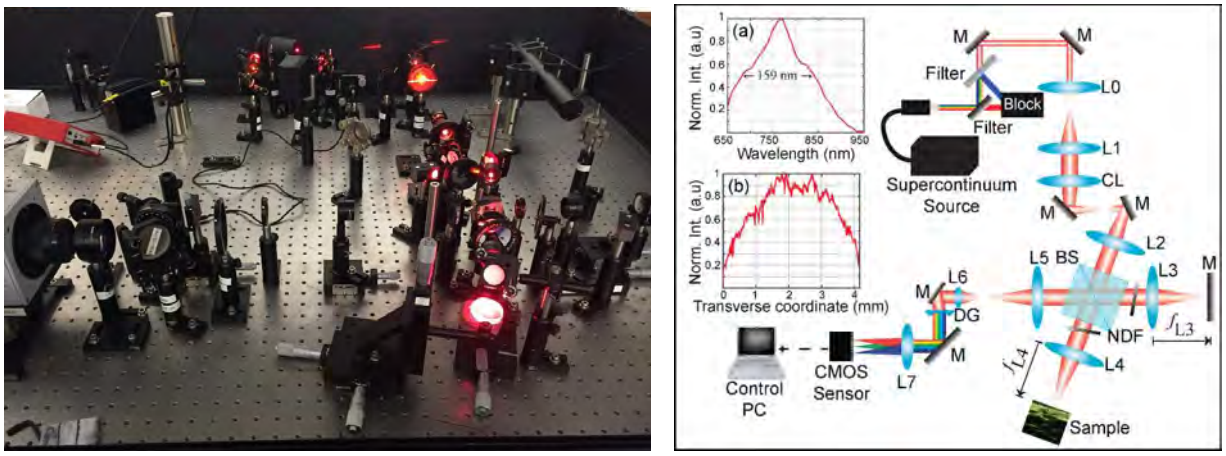

Fig. 2. Left: Photograph of the parallel OCT system. Right: system schematic. M, mirror; NDF, neutral density filter; L, lens; BS, beam splitter. Panel (a) plots the beam's spectrum and (b) its transverse intensity distribution.

What distinguishes this system from previous OCT implementations is the use of a supercontinuum light source (NKT Photonics) to provide nearly 500 mW of continuous-wave illumination within a 650 – 950 nm wavelength band. Because this illumination power is spread over a 6 mm line, it does not significantly perturb biological samples. Yet, the high power provides extremely high SNR (113 dB), while the broad bandwidth enables ultrahigh axial resolution (2 μm). In combination with the 1 kHz frame rate, this system provides an

unprecedented combination of speed, resolution, and sensitivity. Our manuscript describing this system (Barrick et al., 2016), published in *Optics Letters*, was the editor's top pick and the second most popular download in the month it was published.

As a validation of the unique capability of this system, we imaged an *in vitro* model of the human lung epithelium, which has a highly ciliated surface that acts to transport mucus. The periciliary layer is typically only ~7 μm thick, while light scattering fluctuations from the ciliary beating can exceed 100 Hz. As shown in Fig. 3, our parallel OCT system resolves locations of ciliary beating within the periciliary layer, and enables quantification of the median frequency (f_m) of the ciliary beating pattern. This high speed capability enables the high tissue volume scan rates needed for magnetoreceptor detection.

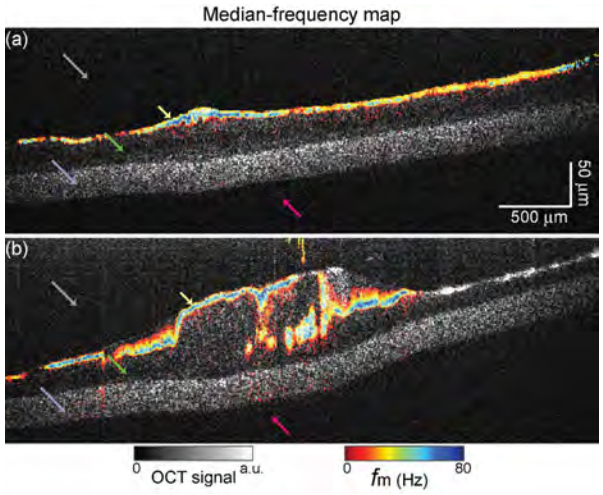

Fig. 3. Dynamic OCT imaging using the median-frequency map (f_m) for two human bronchial-epithelial cell cultures (a) without mucus and (b) with mucus. Colored arrows indicate the different layers of the culture (from top down these layers are: air, periciliary layer, cell layer, porous membrane, and media).

Construction of the Magnetic Field Delivery System

A magnetic field delivery system was constructed and coupled with the parallel OCT system to convert it to a MMOCT system. The electromagnet was comprised of a water-cooled solenoid coil wound on a "bobbin" made of a high-temperature, non-conducting plastic. The electromagnet was mounted to the optical table so that it was mechanically decoupled from the imaging sample, which rested on a glass slide and was imaged with OCT from above (Fig. 4).

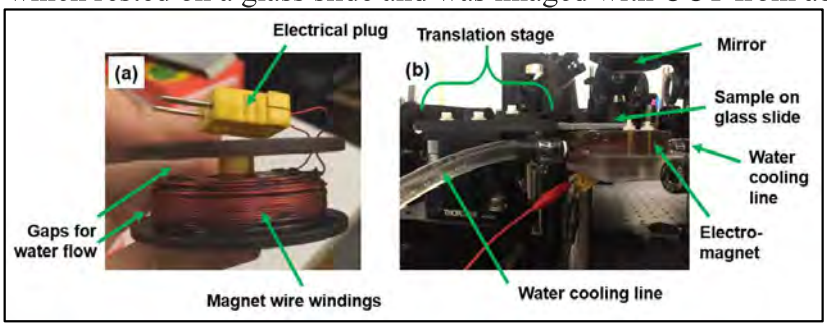

Fig. 4. Photographs of the magnetic field delivery system. (a) Solenoid windings of the electromagnet before enclosing with the outer housing. (b) Enclosed, water-cooled electromagnet shown in position to deliver a magnetic field gradient via the underside of a slide-mounted sample. At the same time, OCT is performed via the parallel line-field light beam reflected from a mirror above the sample. The translation stage performs motorized scans of the sample in *y* to enable volumetric scanning of the OCT *x*-*z* frames.

The primary consideration in designing the electromagnet was to provide a large magnetic gradient force within the imaging region, which is proportional to the dot product of the magnetic field and its gradient, $\vec{B}\cdot\nabla\vec{B}$ (typically reported in Tesla^2/meter, T^2/m). The challenge is that, to perform *parallel* MMOCT, it is necessary to position the magnet on the *opposite* side of the imaging beam because the beam is wider with its line focus. The performance characteristics of the new magnet are summarized in Fig. 5, where this new design is compared to our existing (point-scanning) MMOCT system. The addition of a ferrite core significantly improves performance, especially in the 6 – 10 mm imaging range where the sample is typically located relative to the magnet's top surface.

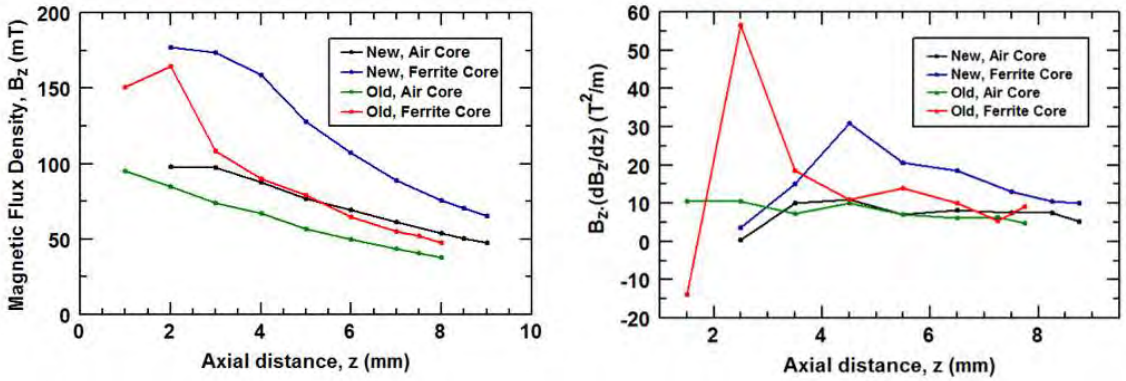

Fig. 5. Plots of new electromagnet performance compared to that of the point-scanning MMOCT system. Left: Axial component of magnetic field vs. axial distance along the solenoid's center line. Right: Magnetic gradient force term, $\vec{B}\cdot\nabla\vec{B}$, computed from the data on the left. Performance is compared with or without use of a high permeability material (ferrite) placed into the core of the electromagnets.

Optimization and Characterization of the Line-field MMOCT system

The MMOCT system offers flexibility in the choice of optical framerate (f_s), magnetic field modulation frequency (f_{mag}), and total number of frames collected (N). Each of these affects the magnetic signal and the background noise. Jessie Barrick's analysis (reported in her PhD thesis) shows that the magnetic signal, S_m, only depends upon the physical vibration amplitude of the particle times the total number of frames collected, N. In practice, N is given by the number of frames per magnet cycle, m, and the total number of magnet cycles recorded, P, such that $N = m*P$. To assess this theory in practice, we studied the effect of m and P individually on S_m (while keeping the other constant). Results are shown in Fig. 6, demonstrating that indeed the magnetic signal scales linearly with each parameter individually. However, it is important to note that the noise also increases approximately as the square root of each parameter.

These results allowed us to optimize the scan parameters. The magnetic signal is linear in N while the noise increases sub-linearly with increasing N. Thus, the highest magnetic signal-to-noise ratio (SNR) is achieved with the highest possible N, which is dictated by practical constraints. The most limiting constraint on N is the total imaging time, T. To prevent overheating the solenoid, T is limited to 1-2 seconds. Given fixed T, N is fixed by the choice of f_s. To maintain an optical SNR > 100 dB, an exposure time of 1 ms is used, which limits f_s to 1 kHz. Given the choice of f_s and a maximum T of 1 second, N is 1000. The choice of P is limited by the desired bandpass filter width to avoid noise contributions non-local to f_{mag}, and thus $P >$ 10 is desirable. To meet the Nyquist sampling criterion for sampling particles modulating at f_{mag}, m must be > 2. Larger m yields a larger dynamic range for the measured displacements, which may not be important for magnetoreceptor detection (this may be at the limit of the system's

displacement sensitivity). The only remaining image acquisition parameter to choose is f_{mag}; to optimize for scan speed, we recommend the highest f_{mag} possible (40 Hz) that avoids B-field losses due to inductance from ferrite core. This leads to an optimized set of imaging parameters as f_s = 1000 Hz, f_{mag} = 40 Hz, and N = 1000, corresponding to m = 25 and P = 40.

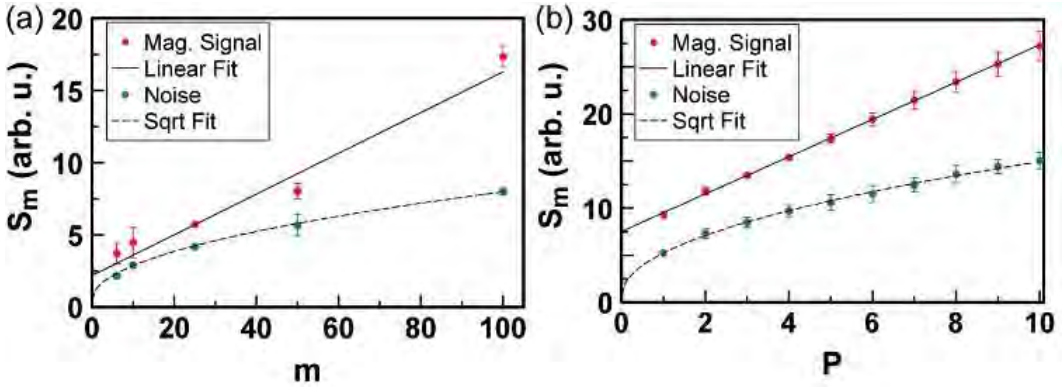

Fig. 6. Effect of (a) temporal sampling, m, and (b) number of magnet cycles, P, on the magnetic signal, S_m when the magnetic field is on (red circles) and when the magnetic field is off (green circles). The linear fit (solid lines; R^2 = 0.97 for (a) and R^2 = 0.99 for (b)) and square root fit (dashed lines; R^2 = 0.99 for both) are performed with an arbitrary offset.

Using this optimized line-field MMOCT system, we measured the Fe sensitivity in elastic, tissue-mimicking samples containing controlled amounts of magnetite (Fe_3O_4) nanopowder. Aqueous tissue-mimicking samples were made of agarose (4.5 mg/g), TiO_2 powder (4.1 mg/g) for optical scattering contrast, and varying concentrations of Fe_3O_4 nanopowder for magnetic contrast, including control. With $p < 0.05$, we found a concentration of 35 µg Fe per gram sample to be distinguishable from the control sample. This is similar to the sensitivity obtained with the prior, line-scanning MMOCT system (Table 1). However, with this new parallel design, we now have over 20 x faster tissue volume scan rate, and also improved optical resolution. The improved resolution is expected to offer greater sensitivity to individual magnetoreceptors. This sensitivity was tested by performing a study in samples with individual magnetic beads, described in the next section.

MMOCT system improvements over the course of the grant

Progress Year	System hardware	Axial resolution	Transverse resolution	Frame size (x × z)	OCT framerate	MMOCT scan method	Magnet frequency	MMOCT framerate	Fe sensitivity	Tissue volume scan rate
past	Prior MMOCT	3 µm	12 µm	2.5 × 1.5 mm	0.25 fps	line	100 Hz	0.125 fps	27 µg Fe/g	5.6 nL/s
Y3				0.5 × 1.5 mm	108 fps	frame	10.8 Hz	0.5 fps	20 µg Fe/g	4.5 nL/s
Y3	Parallel OCT	2 µm	14 µm	4 × 0.5 mm	1000 fps	-	-	-	-	-
Y4	Parallel MMOCT	2 µm	7 µm	5 × 0.5 mm	125 fps	frame	12.5 Hz	0.5 fps	<360 µg Fe/g	8.8 nL/s
Y5					1000 fps	frame	100 Hz	10 fps	<80 µg Fe/g (TBD)	175 nL/s
					1000 fps	frame	10 Hz	1 fps	35 µg Fe/g	17.5 nL/s
Y6					1000 fps	frame	40 Hz	8 fps	35 µg Fe/g	140 nL/s
future					1000 fps	volumetric	100 Hz	25 fps	(TBD)	438 nL/s

Table 1. Progress in OCT and MMOCT system characteristics over the course of the grant. The highlighted cells indicate the optimized system that we completed characterizing, however, a future step in performing volumetric scanning may further improve tissue volume scan rates, if needed.

MMOCT imaging of isolated magnetic beads embedded in soft media

Graduate students Jessica Barrick and Ben Levy analyzed the solution to the vibration of a solid magnetic sphere embedded within a linearly-elastic, homogeneous, isotropic, inviscous, incompressible, elastic medium subject to a sinusoidal external force. They found that within the range of conditions likely to be encountered in realistic MMOCT imaging scenarios, the quasi-static approximation may be used, and the vibration amplitude of the sphere is equivalent to the solution for the displacement of the sphere, u, under a static force, given by:

$$u = \frac{F}{6\pi\mu R},$$

where F is the amplitude of the time-varying magnetic gradient force, μ is the shear modulus of the medium, and R is the radius of the solid sphere. The magnetic gradient force depends upon both the applied magnetic field and the properties of the magnetic sphere, which are substituted into the above expression as follows:

$$u = \frac{R^2\chi}{9\mu\mu_0}\nabla|B|^2,$$

where χ is the magnetic susceptibility of the sphere, μ_0 is the magnetic permeability of free space, and B is amplitude of a square root sinusoidally varying magnetic flux density (so that the force itself is a pure sinusoid).

To compare theory with experiment, we employed magnetic microspheres (MMS) of 1.63 μm in diameter and 42% Fe_3O_4 by mass (Bangs Labs MEGB002). We characterized the volume magnetic susceptibility of the MMS to be 1.2 ± 0.2, the magnetic field delivery system (Fig. 5), and the shear modulus of the agarose samples into which the MMS were embedded. This allowed us to estimate the maximum magnetic gradient force on each MMS to be 7.6 pN, and the corresponding theoretical vibration amplitude of the MMS to be 0.05 nm ± 0.01 nm.

MMOCT imaging of MMS embedded in agarose were carried out and example images are displayed in Fig. 7. The average vibration amplitude of MMS was measured to be 0.96 nm ± 0.27 nm. There are several possible reasons that the measured vibration amplitude of individual MMS is significantly larger than the theoretical value of 0.05 nm ± 0.01 nm. First, the shear modulus of the agarose may be lower than estimated as a result of two things: 1) mechanical damage to the agarose from repeated MMOCT imaging, and 2) heating of the agarose from the high-powered line illumination, as these gels are known to significantly soften with increased temperature. Additionally, it is possible that the MMS partially aggregated within the samples, although the size of the bright scatterers within the sample are consistent with the resolution of the system. With an axial resolution of 2.5 μm, multiple sphere aggregates, if they existed, would only contain a small number of 1.6 μm diameter MMS. Given the multiple sources of uncertainty, we consider the measured vibration amplitude to be in reasonable agreement with the theoretical. Importantly, the signals from these beads are well above background, and provide an upper limit on the size of magnetoreceptors that should be detectible by this system in similarly soft tissues.

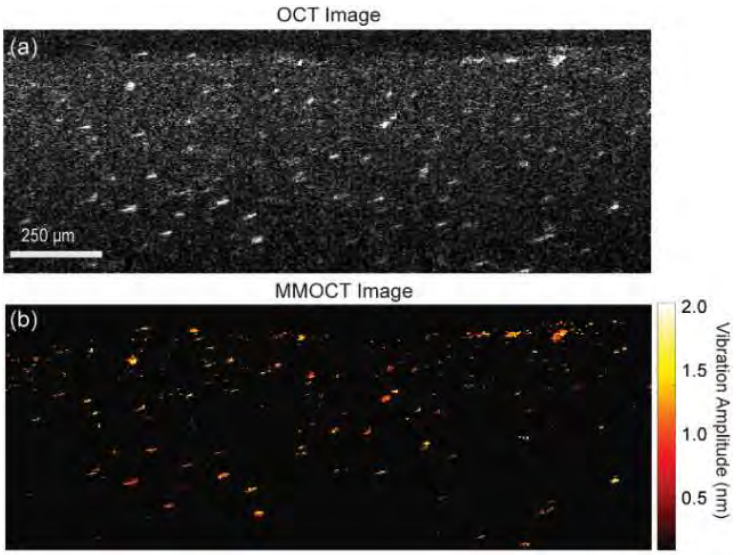

Fig. 7. Representative images of MMS phantom demonstrating single magnetic particle detection with MMOCT. (a) Traditional OCT image; bright points indicate MMS within the agarose gel medium (speckled background). (b) Corresponding MMOCT image, indicating magnetically-induced vibration co-localized with the bright points, as expected.

Preliminary MMOCT Imaging of Biological Magnetite

Graduate student Jessie Barrick collaborated with graduate student Dave Ernst in Ken Lohmann's lab to perform MMOCT imaging of endogenous magnetite crystals. Dave Ernst acquired a solution of magnetotactic bacteria (strain AMB-1) which contain chains of magnetite crystals (see Fig. 8). Bacteria were embedded in gelatin with added optical scatterers (TiO_2) to provide image contrast. Positive and negative controls were imaged alongside samples with the bacteria embedded (Fig. 9).

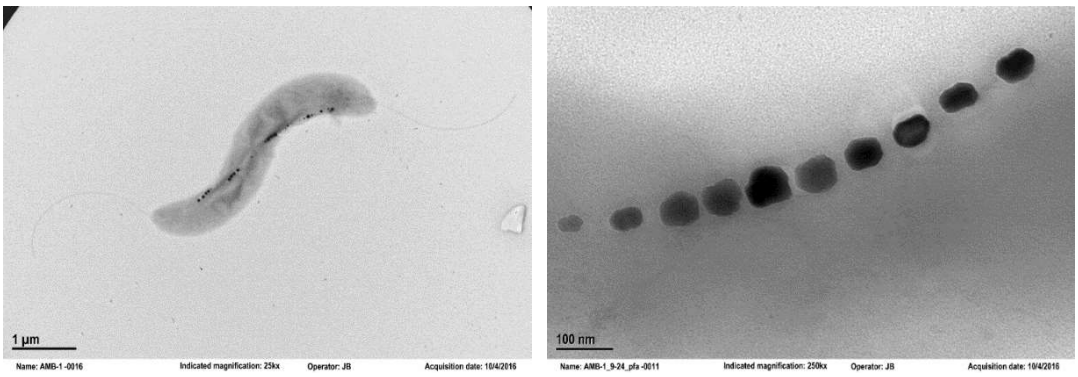

Fig. 8. TEM images of magnetotactic bacteria. Images captured by the Microscopy Services Laboratory at UNC-CH.

We encountered some difficulties with this initial attempt. Some bugs were discovered in the LabVIEW code for acquiring MMOCT data, and the procedure for making the gelatin gels hadn't been optimized for this application. In addition, several different methods for counting the bacteria gave estimates differing by orders of magnitude. We hope to replicate the attempt now that these issues have been resolved. If we succeed, this will represent the first time that endogenous magnetite has been detected using MMOCT, a major step toward our goals.

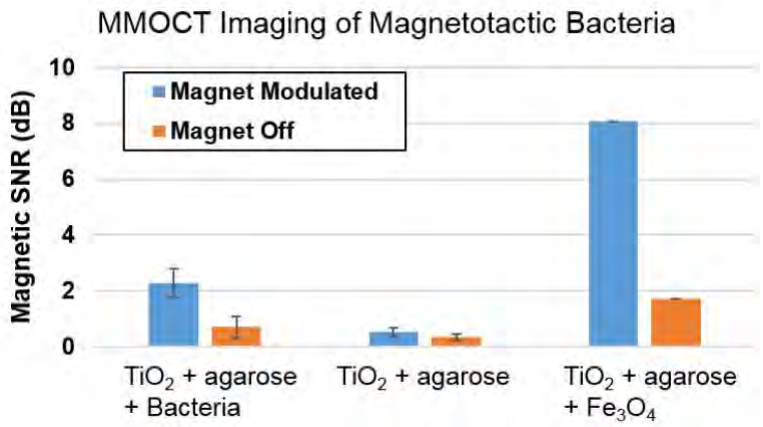

Fig. 9. MMOCT signal from gels containing magnetotactic bacteria (AMB-1), and negative and positive controls with magnetic nanoparticles. The magnetic SNR of the agarose samples for the positive and negative control samples as well as the samples containing magnetotactic bacteria, suggest that the bacteria are producing a measurable magnetic signal. However, the complexities described in the text must be resolved and experiments repeated before a definitive result can be claimed.

Two additional types of samples were imaged by MMOCT to search for evidence of magnetite-based magnetoreceptors (Fig. 10). These were young American eels (glass eel stage) and the larvae of flounder. Eels were fixed with ethanol, and were imaged in the region of the eye, brain, and lateral line. No evidence of magnetomotion was detected. An important caveat, however, is that after ethanol fixation, the eels became less transparent and the imaging depth was superficial (limited to ~0.1 mm of the entire 0.5 mm imaging depth capability). Thus, if magnetite particles were present deeper in the tissue, they might not have been detected under the test conditions. Flounder larvae fixed in ethanol were also imaged in the region of the eye, brain and lateral line. While the flounder larvae samples were more promising in that they offered a greater imaging depth, no significant MMOCT signals were observed in the samples tested. Nevertheless, these initial tests provide a methodology that can potentially be built upon in the future.

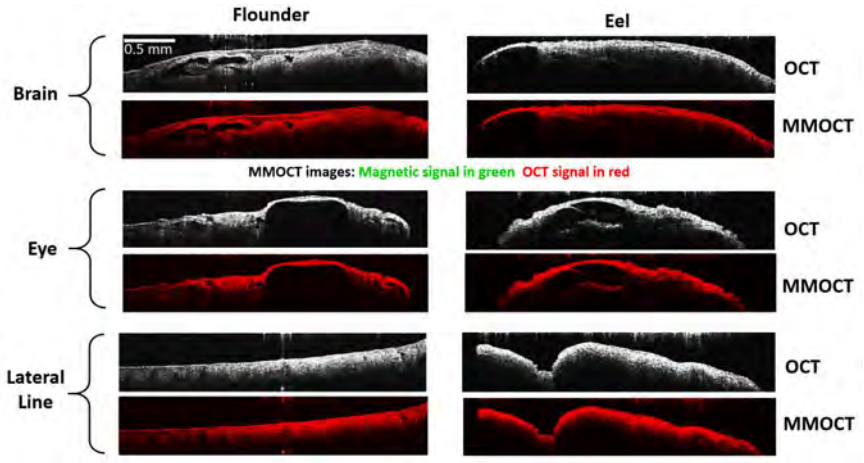

Fig. 10. Representative images of flounder larvae (left) and American glass eels (right). OCT images (black/white) are displayed with their corresponding MMOCT images (red = light scattering, green = magnetic signal). No samples to date have exhibited significant magnetomotive signal.

Summary of MMOCT research

The primary achievement of this portion of the grant was the design and construction of a novel line-field MMOCT system and published papers describing the work. In comparison to MRI, MMOCT provides imaging of magnetic particles embedded in soft media by a completely different contrast mechanism (magnetic gradient-induced motion); the superior resolution of OCT affords higher sensitivity to individual magnetite particles than MRI.

Many undergraduate and graduate students and a postdoc benefitted from support from this grant, including Jessie Barrick who completed her dissertation on the MMOCT system design, and Ben Levy and Diwash Thapa who studied magnetomotion in the context of ultrasonic detection. Complications in the final year of the effort due to Covid 19 led to difficulties in completing the volumetric scanning method and impeded efforts to follow up on promising leads in magnetoreceptor detection. Nevertheless, the new MMOCT system is now available and will be a benefit to future studies in magnetoreceptor detection.

Research Approach 2: Searching for Magnetite-Based Magnetoreceptors Using Transcriptomic Techniques

Approach: Our second research approach involved analyzing changes in gene expression (i.e. transcriptomics) in response to magnetic stimuli. The genes significantly impacted by magnetic stimuli across tissues and species may provide clues about both the location of a magnetoreceptor and its molecular components. The magnetic stimulus used in all experiments was an intense, brief magnetic pulse (~0.08 T, duration 5 ms). Similar magnetic pulses have previously been shown to alter orientation behavior in numerous species. In principle, such pulses can reverse the magnetic dipole moment of a fixed, single domain magnetic particle when applied in the correct direction.

For this work we focused primarily on rainbow trout (*Oncorhynchus mykiss*), although studies using other species of fish (chinook salmon *Oncorhynchus tshawytscha* and American shad, *Alosa sapidissima*) and one invertebrate (the Caribbean lobster *Panulirus argus*) were also conducted. Rainbow trout were a convenient model for magnetoreception for several reasons i) they can be reared in large numbers in a laboratory setting, ii) extensive genomic resources for this species is available, and iii) several studies have documented both a magnetic sense and potentially magneto-sensitive cells in rainbow trout. The general methodology for our transcriptomic studies included exposing individuals to either the magnetic pulse or a sham/mock treatment, followed by tissue dissection and RNA extraction. RNA was sequenced in each sample using Illumina-based next-generation sequencing technologies and analyzed using statistical tools specific to the study depending on the study design, species, and availability of genomic resources.

In addition to the transcriptomic studies introduced above, we completed several studies aimed at further improving our understanding of magnetoreception. These included the development of a new set of statistical tools for modeling animal orientation behavior and a demographic analysis of green sea turtles (*Chelonia mydas*).

Transcriptomics for Rainbow Trout

A total of 251 rainbow trout were exposed to either the magnetic pulse (n = 126) or the mock treatment (n = 125) and were utilized for multiple studies outlined below. RNA was purified from the brain (n=32) or retinas (n=24 from 12 fish) and sequenced.

Brain differential expression: In total, we generated more than 473 million sequence reads 125 bp in length and aligned these to the trout reference genome. We identified 181 genes differentially expressed in the brain (Fig. 11), including multiple copies of the gene encoding the middle subunit of the protein *ferritin*. *Ferritin* is the primary iron-sequestering protein within cells and is thus consistent with a magnetite-based response to a magnetic pulse. A large number of differentially expressed genes were also consistent with effects on gated ion channels or signaling activity, both compatible with the magnetite hypothesis (Table 2). Furthermore, we identified several genes (e.g. *crggm3, purp, prl, gcip, crabp1* and *pax6*) with well-documented associations to the retina and/or optic nerve development and regeneration. These findings suggest the possibility of an effect on visual structures within the brain, for example encephalic photoreceptors of the pineal gland.

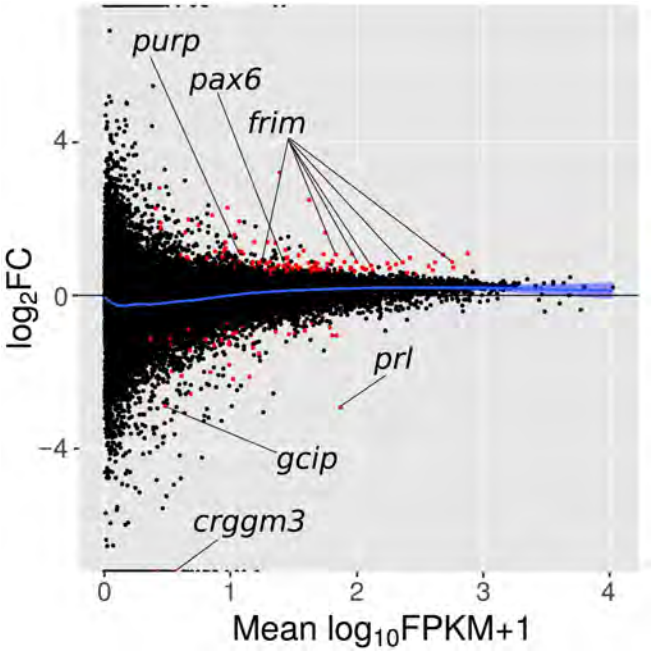

Fig. 11. MA-plot of the expression level (log_{10}FPKM+1) and ratio (log_2FC) for each gene in the trout genome. Comparisons were made between control trout and those exposed to a magnetic pulse. Genes with significantly different expression are shown in red. A smoothed function generated using a generalized additive model is provided (blue line). Candidate genes are listed, noticeably six copies of the middle subunit of the ferritin protein (*frim).* From Fitak et al. (2017, *Biol. Lett.*).

Calcium ion activity	Sodium ion activity	GTPase activity	Glutamate activity	Iron ion/oxidoreduction	Visual structures
clstn1	*slc6a1*	*mmaa*	*gad2*	*tecr*	*prl*
prv7 (x2)	*slc6a9*	*arhgap40*	*grin2c* (x2)	*scd*	*gcip**
*gcip**	*slc1a2*	*arhgap20*	*glul*	*p4ha1*	***crygm3***
trpc1		*arhgap39*	*glrk*	*frim* (x5)	*purp*
casq2		*pkp4* (x2)	*grin1a*	*sod1*	*crabp1*
anxa1		*rabep1*			*pax6*
fat4		*rabgef1*			*col2a1*
pvalb4		*rash*			
pkd2		*rims1*			
actn3		*sntxa*			
		atl2			
		ccdc136			
		tub1a1			

**gcip* both binds calcium ions and is found in photoreceptor cells

Table 2. Genes differentially expressed in the trout brain and retina by a magnetic pulse that are consistent with the various pathways predicted by a hypothetical magnetite-based magnetoreceptor or with visual structures and pathways. The gene *crygm3* (bold) was found in both brain and retina tissues, and genes identified from re-analyzing the unmapped sequencing reads in the trout brain (Arniella et al. 2018 *Env Biol Fishes*) are shown in red.

We also analyzed the sequences that failed to align to the existing trout reference genome. These sequences represent regions missing, misassembled, or divergent from the reference genome and may contain additional candidate genes affected by the magnetic pulse. A total of 27 million sequences from our initial study of the brain did not align to the reference genome, and were re-assembled into a new reference transcriptome. From the new reference transcriptome, which contained 45,142 contigs, we identified 12 that were differentially expressed after the magnetic pulse, including six up-regulated and six down-regulated (Fig. 12). Three of the differentially expressed contigs could not be annotated with a known gene or function. Two additional contigs, identified as an unnamed (uncharacterized) protein with calcium ion binding activity in the cellular membrane and *tubulin alpha chain* were down-regulated by the magnetic pulse. These two genes, with active roles in ion signaling and cytoskeleton organization, are consistent with the release of calcium ions triggered by torsion on the cytoskeleton predicted by magnetite-based magnetoreception (Table 2). The largest effect was a >400-fold reduction in a contig described as *collagen alpha-1 type II*. This structural protein is a component of the vitreous humor of the eye, and mutations in this gene are responsible for Stickler syndrome type I, a disease that causes retinal detachment and degeneration in humans. Finally, the magnetic pulse resulted in a 32-fold decrease in the gene coding for *superoxide dismutase*. *Superoxide dismutase* neutralizes the superoxide radical thus preventing oxidative damage to cells. Taken together, the results from this study were congruent with our previous work, demonstrating effects consistent with magnetite-based magnetoreception but also a potential role for encephalic photoreceptors (Table 2).

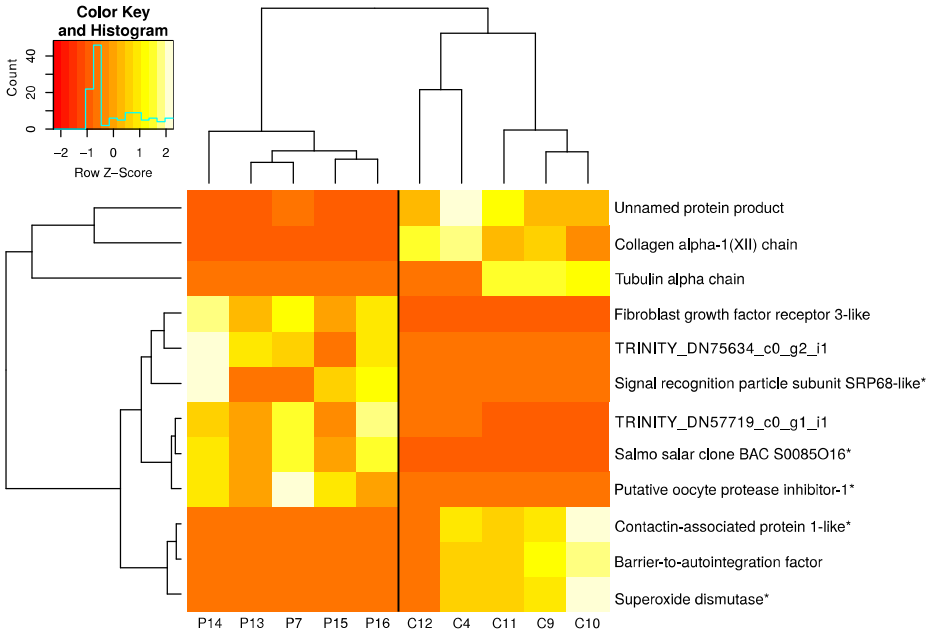

Fig. 12. Heatmap of the differential expression results. Each box represents the raw counts of sequences aligned to that contig normalized to the mean counts across all samples (Row Z- Score) and colored according to the scale provided. Unlike $\log_2$FC, which is calculated across all samples for a gene, the Z-score is a metric to visualize expression within samples. Both the rows (contigs) and RNA-seq libraries (columns) are hierarchically clustered based upon Euclidean distances (P = pulsed libraries, C = control libraries). The 10 libraries shown are identical to those used for differential expression in Fitak et al. (2017). Asterisks indicate contigs assigned annotation only by BlastN and not using Blast2Go.

Retina differential expression: Because the initial results suggested a potential role for visual structures and/or pathways, we examined the expression of genes in the retina of rainbow trout after exposure to the same magnetic pulse (Fitak et al. 2018 *Biol Lett*). Both left and right retinas were analyzed separately in light of a previous report suggesting the possibility of lateralization of a magnetic sense. We sequenced RNA libraries generated from both the left and right retina of six control and six pulse-magnetized fish (24 libraries in total). This study also included a reference-guided assembly to identify possible differential expression among other types of RNA molecules (e.g., long non-coding RNAs), poorly assembled genomic regions, and splice variants (Fig. 13). Differential expression was calculated using a combination of methods to avoid concerns of missing potential effects in sequences that fail to align to the reference genome and leveraging the strength of linear models to describe the interaction of effects between treatments (control vs. pulsed) and eyes (left vs. right).

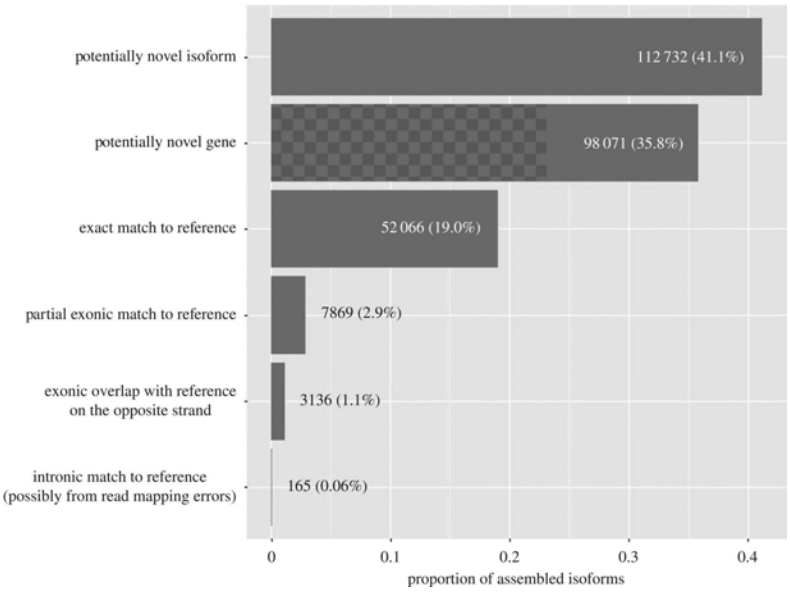

Fig. 13. Distribution of contigs generated by the reference-guided assembly from the trout retina and compared with the reference genome. The checkered area represents contigs matching to known long non-coding RNAs.

In summary, we generated >1.2 billion paired-end sequences, but identified no evidence for lateralization of expression (without regard to the magnetic pulse) nor an effect of the pulse within each retina when analyzed independently. However, when analyzed using a modeling approach to account for an interaction between lateralization and the magnetic pulse, a single gene, *gamma-crystallin M3-like*, was differentially expressed (Fig. 14). Interestingly, this gene, which is a major component of the vertebrate lens, was also differentially expressed in the brain after exposure to the magnetic pulse (Table 2). These results showed that a magnetic pulse has little to no effect on gene expression in the retina, indicating the brain (or other tissues not yet examined) represents a more likely location of a magnetoreceptor. The results also imply that the magnetic pulse does not produce generalized effects on neurological tissue.

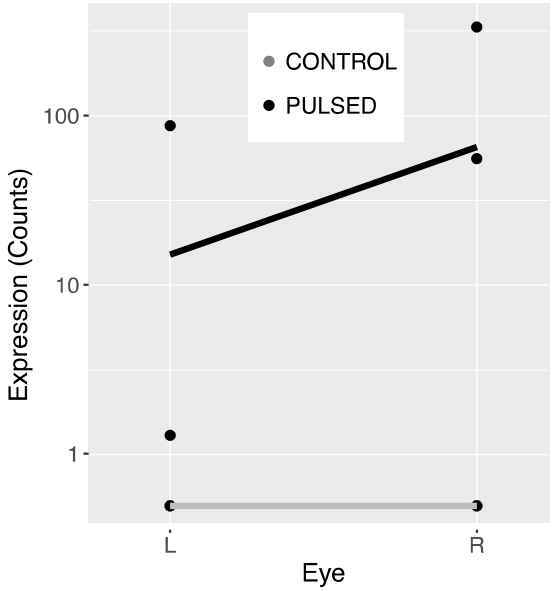

Fig. 14. Effect of the magnetic pulse on *g-crystallin M3-like*. The mean expression in control (gray line) and pulsed (black line) fish. No expression was observed in all control fish.

Candidate Gene Studies: Chinook Salmon and American Shad

Additional studies included the development and use of an assay to examine the expression of a panel of our candidate genes in Chinook salmon and American shad, two fish that migrate long distances. The study of Chinook salmon was performed in collaboration with researchers at the Oregon Hatchery Research Center. A total of 160 juvenile Chinook salmon were exposed to either the magnetic pulse or control treatment, and the brain and eyes of each individual were harvested at either 10 min, 30 min, 1-hr, 3-hr, 6-hr, 12-hr, 24-hr, or 48-hr post treatment. All RNA extractions from the brain were completed and assessed using an Agilent RNA ScreenTape assay with the Agilent 2200 TapeStation system. The RNA integrity number (RIN) for all samples was >8.4 (on a 1-10 scale), indicating all RNA samples were of high quality and integrity with minimal degradation.

We developed an assay to quantify the expression of 23 candidate magnetoreception genes using the Nanostring nCounter system. The Nanostring technology provides a highly sensitive, reproducible system of quantifying expression directly from RNA rather than after reverse transcription into cDNA. Furthermore, the recent publication of the Chinook genome sequence allowed us to design oligonucleotide probes specific to this species. The expression assay, called a "codeset", was developed and run in two phases. In phase 1, we worked in three stages to develop, optimize, and test *in silico* the codeset. This codeset is called *Fitak_Otsh* and can be purchased from Nanostring. We used the codeset *Fitak_Otsh* to assay the expression of half (n=80) of the brain RNA extractions from Chinook salmon. In phase II, we developed a new version of the codeset, called *Fitak_Otsh_v2* based on the results from phase I. In all, the expression levels of three genes from phase I (*TFR2*, *HAMP*, and *CRYGM3*) were not much above background, and were thus replaced with three genes (*KLF11*, *ARHGAP40*, and *ANXA1*) differentially expressed in brain tissue from our previous study (Fitak et al. 2017 *Biol Lett*). A complete summary of the 23 genes assayed by the codesets are shown below in Table 3.

	Accession (*O. tshawytscha*)	Symbol	Description	Reason for inclusion
1	XM_024373666.1	IREB1	aconitase 1	Iron homeostasis pathway
2	XM_024379022.1	CRABP1	cellular retinoic acid binding protein 1	Differentially expressed
3	XM_024379018.1	IREB2	iron responsive element binding protein 2	Iron homeostasis pathway
4	XM_024379813.1	CRY1	cryptochrome-1-like	Chemical magnetoreception
5	XM_024388824.1	SLC40A1	solute carrier family 40 member 1-like	Iron homeostasis pathway
6	XM_024391788.1	TF2	serotransferrin	Iron homeostasis pathway
7	XM_024392128.1	TFR1	transferrin receptor protein 1-like	Iron homeostasis pathway
8*	XM_024392248.1	TFR2	transferrin receptor protein 2-like	Iron homeostasis pathway
9	XM_024392873.1	RPS20	40S ribosomal protein S20	Housekeeping gene
10	XM_024396038.1	EF1a	elongation factor 1-alpha, oocyte form-like	Housekeeping gene
11	XM_024400305.1	SOD2	superoxide dismutase [Mn], mitochondrial	Differentially expressed
12	XM_024405169.1	CYBRD1	cytochrome b reductase 1-like	Iron homeostasis pathway
13	XM_024409124.1	B-actin	actin, cytoplasmic 1-like	Housekeeping gene
14*	XM_024413016.1	HAMP	hepcidin	Iron homeostasis pathway
15*	XM_024413871.1	CRYGM3	gamma-crystallin M3-like	Differentially expressed
16	XM_024417794.1	PURP	purpurin-like	Differentially expressed
17	XM_024423342.1	PRL	prolactin	Differentially expressed
18	XM_024427521.1	NRAMP2	natural resistance-associated macrophage protein 2-like	Iron homeostasis pathway
19	XM_024432773.1	Frim	ferritin, middle subunit-like	Iron homeostasis pathway
20	XM_024436528.1	HERC6	E3 ISG15--protein ligase HERC5-like	Differentially expressed
21	XM_024436632.1	VPS37C	vacuolar protein sorting-associated protein 37C-like	Differentially expressed
22	XM_024438158.1	ZIP14	zinc transporter ZIP14-like	Iron homeostasis pathway
23	XM_024418120.1	MRPS27	mitochondrial ribosomal protein S27	Differentially expressed
24**	XM_024429818.1	KLF11	Krueppel-like factor 11	Differentially expressed
25**	XM_024439199.1	ARHGAP40	rho GTPase-activating protein 40-like	Differentially expressed
26**	XM_024439306.1	ANXA1	annexin A1-like	Differentially expressed

*Included in phase I (codeset *Fitak_Otsh*), excluded in phase II for low expression
** Added in phase II only (codeset *Fitak_Otsh_v2*)

Table 3: List of the genes (according to RefSeq accession numbers in the *O. tshawytscha* genome) included in the Nanostring custom codesets.

The expression results are summarized below. For phase I, the expression levels of 80 brain RNA isolates from Chinook salmon were assayed using codeset *Fitak_Otsh*. These 80 samples represent five biological replicates from each timepoint for both control and pulse-magnetized individuals (Table 4). Of the 80 samples, seven were randomly selected and triplicated across batches (each codeset analyzes batches of 12 samples) to serve as technical replicates for estimation of the precision (coefficient of variation, CV). An additional two no-template-control (NTC) samples were included, for a grand total of 96 expression assays in phase I.

Time point	Group	N (phase I)	Technical Replicates, phase I (CV ± SD)	N (phase II)	Technical Replicates, phase II (CV ± SD)
10 min	CONTROL	5		5	
	PULSED	5		5	
30 min	CONTROL	5	1 (4.3% ± 5.0%)	5	
	PULSED	5		5	1
1 hr	CONTROL	5	1 (4.9% ± 5.8%)	5	
	PULSED	5		5	1
3 hr	CONTROL	5		5	
	PULSED	5	1 (7.9% ± 7.2%)	5	1*
6 hr	CONTROL	5		5	
	PULSED	5	1 (8.3% ± 9.4%)	5	1
12 hr	CONTROL	5		5	
	PULSED	5		5	

24 hr	CONTROL	5	1 (12.7% ± 22.3%)	5	1*, 1
	PULSED	5	2 (12.0% ± 14.6%) (7.6% ± 6.4%)	5	1*
48 hr	CONTROL	5		5	
	PULSED	5		5	
NTC	N/A	2		2	

*samples replicated from phase I also

Table 4: Summary of the sample groups and replicates for phase I and phase II of the Nanostring expression study. CV = coefficient of variation, or precision of the technical replicate across 20 assayed genes; SD = standard deviation.

All raw expression data were reported as counts, which were subsequently normalized relative to the geometric mean of the three housekeeping genes shown in Table 3. These housekeeping genes were selected based upon previous quantitative PCR studies in salmonids, an additional Nanostring study in Chinook salmon using different genes, and the observation that these genes were highly expressed in our previous brain study without detectable effect of the treatment. The analysis includes a spike-in positive control standard curve for each sample, which produced an overall $R^2 \geq 0.99$ (Fig. 15A). Built-in negative controls provided by Nanostring and the two NTC samples passed all quality control benchmarks and determined the lower limit of detection which was subtracted from all sample measurements. All three housekeeping genes had a CV < 1 (Fig. 15B) which is indicative of a low variance dataset and robust for expression normalization. Among the seven triplicated technical replicates of phase I, the overall mean CV, or precision, across the 20 assayed genes (excluding the housekeeping genes which were used for normalization) was 8.2% ± 6.3%. This precision was well below the maximum recommended threshold of 11% for expression studies, and indicative of reproducible results.

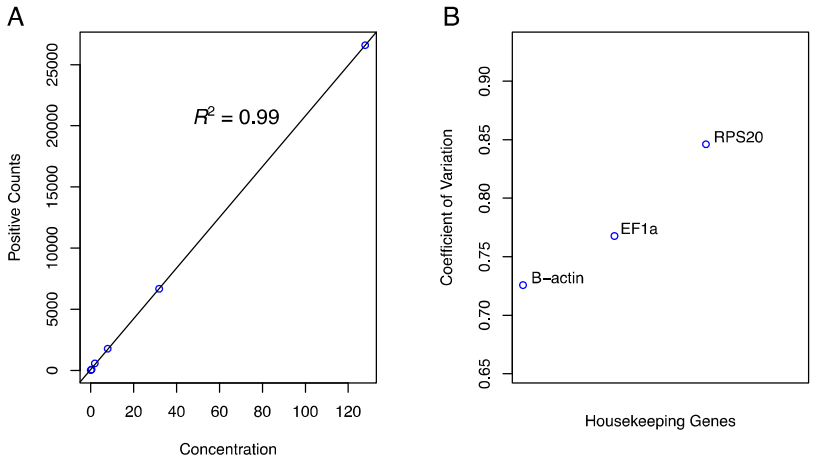

Fig. 15: (A) Spiked-in positive control expression (counts) as a function of the concentration. The mean across samples is shown for each point. (B) The coefficient of variation (CV) for the three housekeeping genes.

In Fig. 16 below, the normalized, relative expression of each of the 20 assayed genes is presented. In general, the expression patterns were quite variable, with noticeable increases in expression after exposure to the magnetic pulse in 5 genes (i.e., *frim*, *HERC6*, *IREB2*, *CYBRD1*, and *MRPS27*) starting approximately 24 – 48-h post-exposure.

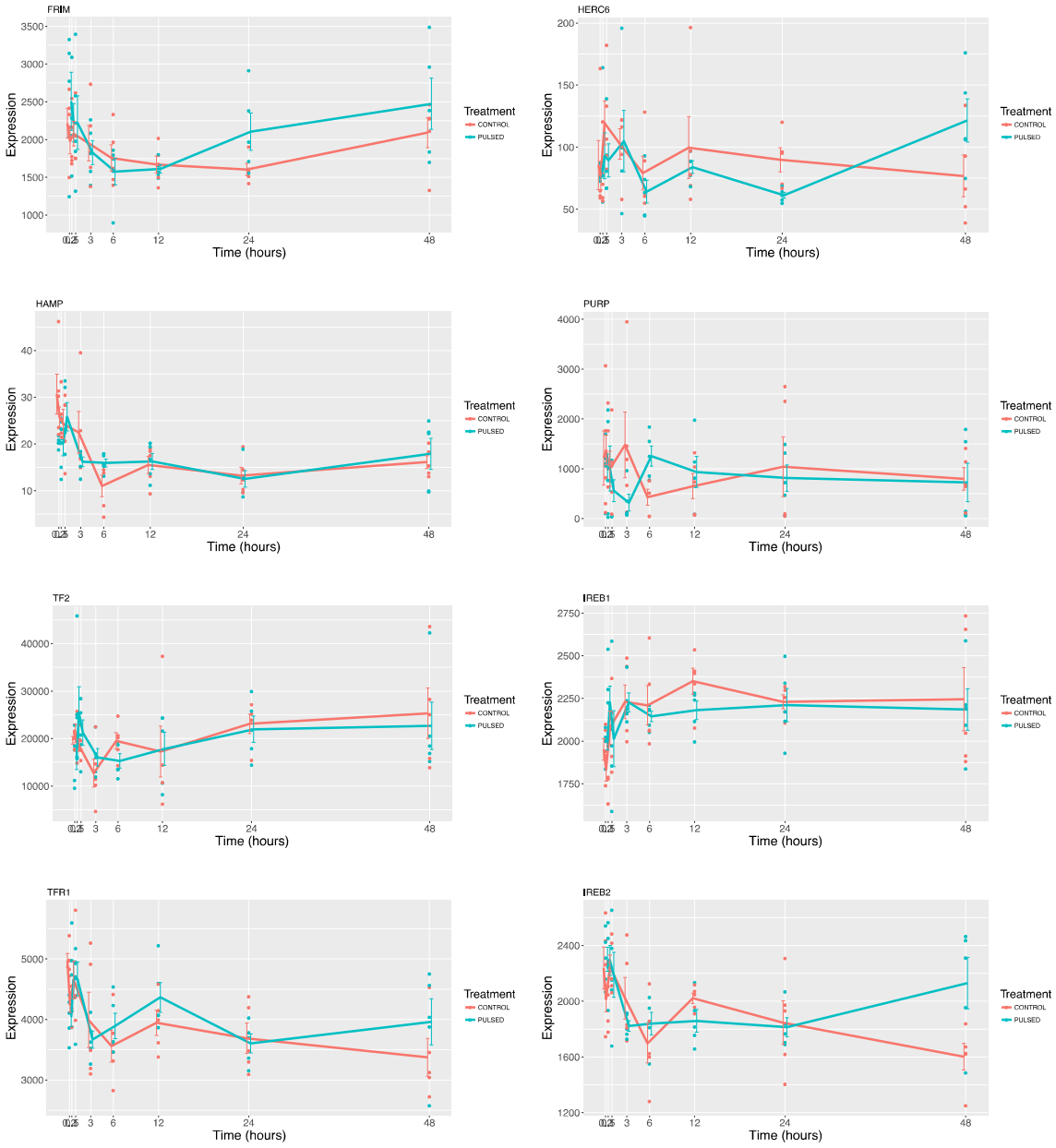

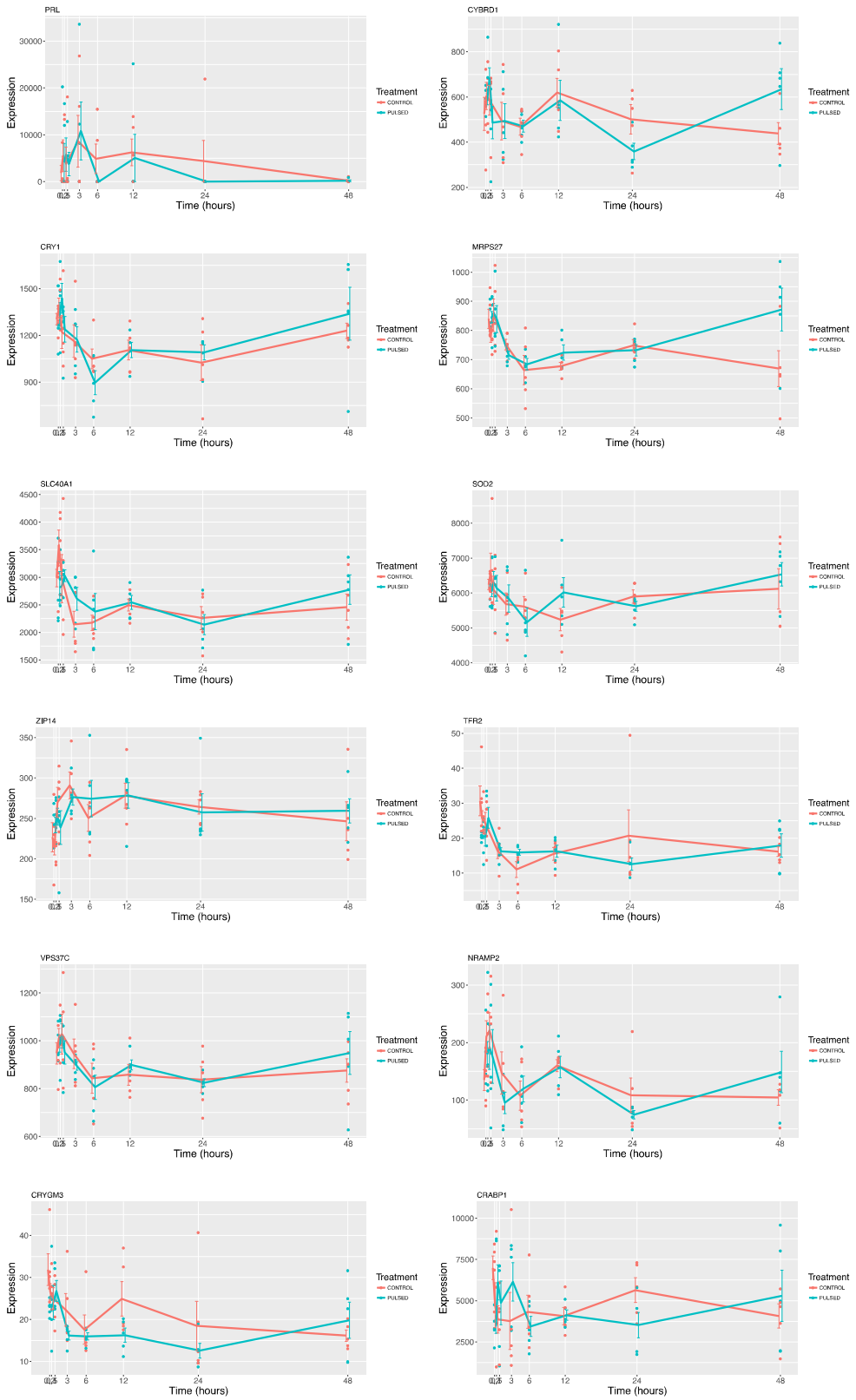

Fig. 16. Normalized expression counts for each gene (plotted separately). The gene symbol is provided in the upper left (see Table 2 for a gene description). Only the results from phase I are shown.

To statistically test for differential expression between control and pulsed individuals across time points, we used the R package "NanoStringDiff" v1.9.2 (Table 4). This method models the expression count data using a generalized linear model of the negative binomial family. The model framework includes a normalization based upon positive controls, negative controls, and the housekeeping genes. An empirical Bayesian shrinkage technique is used to estimate the dispersion parameter and a likelihood ratio test is employed to detect differentially expressed genes. In our study, we modeled expression, y, as

$$y \sim 0 + group + RNA$$

Where $group$ is a factor formed by combining the treatment (control vs pulsed) with the appropriate time point (e.g., 10 min) and RNA is a continuous predictor of the RIN and thus accounts for varying RNA quality among samples. Likelihood ratio tests were performed for each of the 20 genes for each timepoint of phase I and p-values were calculated and corrected using a false discovery rate threshold of 0.05.

Gene	10 min	30 min	1 hr	3 hr	6 hr	12 hr	24 hr	48 hr
CRABP1	-0.98 (0.009)	0.37 (0.166)	0.17 (0.277)	0.66 (0.047)	-0.31 (0.271)	0.06 (0.41)	-0.66 (0.072)	0.37 (0.209)
CRY1	0.07 (0.602)	0.06 (0.677)	0.04 (0.777)	-0.03 (0.847)	-0.21 (0.131)	0.04 (0.789)	0.13 (0.37)	0.1 (0.459)
CRYGM3	-0.11 (0.036)	-0.02 (0.505)	0.04 (0.052)	**-1.24 (0.003)**	-0.8 (0.049)	-1.24 (0.037)	-1.16 (0.009)	0.57 (0.151)
CYBRD1	0.22 (0.281)	0.2 (0.345)	-0.05 (0.681)	-0.04 (0.736)	-0.04 (0.729)	-0.04 (0.739)	-0.55 (0.014)	0.55 (0.012)
Frim	0.22 (0.248)	0.17 (0.387)	0.08 (0.655)	-0.12 (0.506)	-0.16 (0.414)	-0.02 (0.779)	0.46 (0.024)	0.2 (0.295)
HAMP	1.33 (0.324)	-17.75 (0.039)	-1.89 (0.317)	-19.63 (0.095)	-4.19 (0.322)	0.73 (0.365)	-16.56 (0.27)	15.61 (0.148)
HERC6	-0.07 (0.558)	0.17 (0.396)	-0.39 (0.179)	0.04 (0.486)	-0.41 (0.189)	-0.23 (0.346)	-0.38 (0.238)	0.88 (0.007)
IREB1	0.08 (0.445)	0.27 (0.007)	0.07 (0.533)	-0.03 (0.751)	-0.04 (0.687)	-0.07 (0.459)	0.04 (0.665)	-0.07 (0.473)
IREB2	0.09 (0.399)	0.18 (0.077)	0.1 (0.407)	-0.2 (0.06)	0.13 (0.241)	-0.08 (0.425)	0.01 (0.954)	**0.39 (0)**
MRPS27	0.06 (0.474)	0.14 (0.144)	0.05 (0.624)	-0.15 (0.175)	0.07 (0.541)	0.13 (0.198)	0.05 (0.675)	**0.39 (0)**
NRAMP2	0.49 (0.107)	-0.12 (0.312)	-0.05 (0.366)	-0.72 (0.048)	0.1 (0.41)	0.02 (0.382)	-0.67 (0.05)	0.66 (0.051)
PRL	**1.25 (0)**	**0.08 (0)**	**0.31 (0)**	**0.19 (0)**	**-8.96 (0)**	**-0.15 (0)**	**-7.63 (0)**	**-0.31 (0)**
PURP	**-0.2 (0.001)**	-0.42 (0.063)	-0.96 (0.156)	**-2.26 (0)**	1.55 (0.022)	0.55 (0.076)	-0.35 (0.005)	-0.21 (0.016)
SLC40A1	-0.04 (0.79)	-0.35 (0.031)	0.08 (0.64)	0.24 (0.147)	0.12 (0.455)	0.06 (0.693)	-0.04 (0.812)	0.15 (0.362)
SOD2	0 (0.877)	-0.07 (0.52)	0.04 (0.775)	0.01 (0.861)	-0.11 (0.32)	0.24 (0.028)	-0.03 (0.765)	0.06 (0.569)
TF2	-0.25 (0.302)	0.26 (0.328)	0.16 (0.454)	0.3 (0.249)	-0.35 (0.186)	0.1 (0.543)	-0.04 (0.562)	-0.18 (0.514)
TFR1	-0.25 (0.03)	0.13 (0.273)	0.13 (0.296)	-0.15 (0.202)	0.12 (0.33)	0.18 (0.127)	0 (0.926)	0.2 (0.095)
TFR2	0.31 (0.207)	-0.66 (0.082)	-0.86 (0.067)	-0.15 (0.236)	4.94 (0.296)	-1.73 (0.32)	-8.49 (0.177)	9.59 (0.054)
VPS37C	0.11 (0.192)	0.01 (1)	-0.02 (0.8)	-0.11 (0.299)	-0.05 (0.643)	0.1 (0.318)	0.01 (0.94)	0.11 (0.233)
ZIP14	0.16 (0.115)	0.22 (0.026)	0.02 (0.885)	-0.15 (0.207)	0.14 (0.248)	0.03 (0.72)	0.05 (0.719)	0.1 (0.431)

Table 5: Results of the likelihood ratio tests for differential expression for each gene. The values shown are the log fold change in the pulsed relative to control individuals for each time point, with the p-value within parentheses. Items shown in bold-faced type remained significant after false discovery rate correction (<0.05).

Interestingly, the gene encoding the hormone prolactin (*prl*) was consistently differentially expressed across time points. Notably, beginning approximately 6-hrs after pulse exposure, the expression of *prl* was nearly eliminated, resulting in relatively large effect sizes. This result is similar to that we reported previously in the brain of rainbow trout. The function *prl* may play in magnetoreception and/or responding to the magnetic pulse is unclear, although *prl* in fish is known to have a multitude of functions and is perhaps best known for osmoregulation. The gene *purp* was significantly reduced in expression 10-min post-exposure, as we also reported previously in the rainbow trout brain, but this effect was amplified after 3-hrs post pulse exposure. Again, the relationship with magnetic stimulation is unclear, but *purp* (also known as *RBP4*, the retinol transporting protein in blood) concentration in blood is known to directly correlate with iron stores in the blood. Otherwise, significant effects of the pulse were also

observed in *CRYGM3*, *IREB2*, and *MRPS27*. In particular, *IREB2* (iron-responsive element binding protein 2) is of interest as it is a primary, upstream regulator of the iron homeostasis and regulatory pathways. *IREB2* is an important repressor of *frim* (ferritin) when iron levels are low. We concurrently observed a large, albeit nonsignificant, increase in *frim* at 24 and 48 hr after exposure. In all, these results demonstrate that 1) gene expression profiling with Nanostring can produce robust, reproducible results, 2) changes in gene expression resulting from a magnetic pulse can vary widely across a 48-hr window, 3) many changes in gene expression were consistent with those reported previously 10-min post-pulse in rainbow trout, and 4) the magnetic pulse appears to affect cellular iron homeostasis and regulation pathways, and the relationship of this result with magnetoreception needs further explored.

We also repeated the above experiment using American shad. The shad were captive hatched from wild parents collected in the Neuse River by the Edenton National Fish Hatchery. Although it is currently not known whether shad possess a magnetic sense, they share many of the same life history characteristics as salmonids (i.e. anadromous) including natal homing abilities. We exposed 90 shad to either a control or magnetic pulse treatment, euthanized them at various time intervals (10 min, 30 min, 45 min, 1-hr, 1.5-hr, 2-hr, 3-hr, 6-hr, 12-hr), and preserved their tissues for subsequent transcriptomic or genetic analyses. The time intervals differ from the experiment performed in Chinook salmon due to the sensitive and difficult nature of handling the shad in captivity. The downstream expression studies will depend upon the results obtained from the Chinook salmon in order to target specific candidate genes that demonstrate a time-dependent response to the magnetic pulse.

Candidate Gene Studies: Caribbean Spiny Lobster

Magnetoreception exists not only in fish, but in phylogenetically diverse animals. The Caribbean spiny lobster, *Panulirus argus,* is an unusual invertebrate because it is known to have both a magnetic compass and a magnetic map. Thus, as a first step in extending our findings to other species, we investigated transcriptomic responses of lobsters to pulsed magnetic fields (Ernst et al., 2020). Specifically, we examined gene expression in the central nervous system of Caribbean spiny lobsters after applying a magnetic pulse known to alter magnetic orientation behavior (behavioral results are described in the third part of the report).

In lobsters, exposure to the magnetic pulse elicited altered expression of a large number of genes (10.2% of all expressed genes) throughout the central nervous system. Affected genes included some involved with iron regulation, response to oxidative stress, DNA damage and repair, and immune response. These results are consistent with the magnetite hypothesis of magnetoreception, inasmuch as they are compatible with the interpretation that the pulse damaged or altered magnetite-based magnetoreceptors located in the lobster central nervous system. In addition, however, the number and diversity of genes altered by the pulse indicate that a magnetic pulse has effects that are unlikely to be exclusive to magnetoreceptors. A full list of genes with altered expression, and what is known about their function, has now been published (Ernst et al., 2020).

In principle, a magnetic pulse might affect magnetite-based magnetoreceptors through remagnetization (e.g., reversing the magnetic dipole moment of magnetite crystals), physical damage to the receptor as a result of translocation and/or rotation of magnetite particles upon exposure to the strong magnetic gradient produced by the pulse, and/or disruption of clusters of interacting superparamagnetic crystals. For these reasons, we predicted that if such magnetoreceptors exist within the lobster central nervous system, then a magnetic pulse might

induce the expression of genes involved with iron regulation, possibly indicating magnetoreceptor repair or replacement, the deleterious oxidative effects of free iron on cells, and processes related to tissue damage. Analyses revealed that, in each tissue examined, genes linked to iron binding, transport, and homeostasis did indeed have significantly altered expression. Genes linked to oxidative damage and DNA damage/repair also had altered expression. Together, these results provide evidence that the magnetic pulse had an impact on iron homeostasis within the lobster central nervous system, possibly as a result of damage to magnetite-based magnetoreceptors and subsequent repair or replacement of impaired receptors. Additional studies will be needed to determine which of the candidate genes function in magnetoreception.

Although the magnetic pulse had effects consistent with an impact on iron-related processes, genes that serve other functions were also affected, including genes linked to protein synthesis, immune responses, and mitochondria. Thus, although the overall results are consistent with magnetite-based magnetoreception, the fact that magnetic pulses also affected the expression of genes seemingly unrelated to magnetoreception suggests that caution is required when interpreting the effects of magnetic pulses on animal behavior.

<u>New Statistical Procedures and Genomics</u>

In parallel with using transcriptomics to search for magnetoreceptors, we have also developed and implemented new statistical tools for the analysis of magnetic orientation data (Fitak and Johnsen 2017 *J Exp Biol*). In the software *CircMLE*, we described a method through which researchers can mathematically assess and compare the fit of circular models (e.g., uniform, unimodal, bimodal) to their data. The new software is freely available as a package for R. A more rigorous statistical treatment of animal orientation studies will facilitate interpretation of behavioral studies of magnetoreception.

Finally, we used the genome sequence available for green sea turtles (*Chelonia mydas*) to reconstruct their demographic history (Fitak and Johnsen 2018 *Mar Biol*). Our results found a large increase in population size near the last geomagnetic field reversal (the Brunhes–Matuyama reversal) ~800,000 years ago. Using simulations, we showed that this result could possibly be attributed to changes in population structure or gene flow as a consequence of the impacts of the field reversal on their ability to navigate magnetically. Using these results, we have further outlined a framework for using population genomics to infer the relationship between variation (both secular and reversals) in the geomagnetic field and the biogeography of navigating species, a concept we refer to as geomagnetic biogeography.

Research Approach 3: Bio-sensory Basis of Long-range Navigation and Behavioral Assays for Investigating Magnetoreception

Our final research approach involves the first objective of the "Bio-Sensing of Magnetic Fields" BRI, which is to "address the bio-sensory basis for long-range navigation by orientation to the geomagnetic field." For this objective, it is necessary to study magnetic navigation behavior itself, because this represents the final output of the magnetosensory system. In sensory systems, higher-order neural processing (that is, processing that occurs in the brain above the level of receptors) often acts as a filter that discards aspects of the sensory world that are not directly relevant to the task that must be performed. Thus, neural filtering and feature extraction are often at least as important as receptor responses in shaping the motor outputs that comprise behavior. A thorough understanding of magnetoreception thus includes not only identification of

receptors, but an understanding of how magnetic information is used by animals to guide long-range movements, and also knowledge of what specific magnetic parameters the animal uses when making navigational decisions. Work in this area has involved a variety of statistical, behavioral, and modeling approaches, as summarized below.

Evidence for Geomagnetic Imprinting in Sea Turtles

How sea turtles and other marine animals migrate across oceans and then navigate back to the area where they originated has remained an enduring mystery. A major conceptual breakthrough occurred when we realized that large, public databases on sea turtle nesting patterns can be mined to obtain insights into the magnetic parameter(s) that turtles use to navigate to their home beaches. This new technique, which involves detailed statistical analyses on changes in nesting patterns associated with subtle changes in Earth's field, led to a paper published in *Current Biology* (Brothers and Lohmann, 2015). A brief summary of this work follows.

The study investigated natal homing, a pattern of behavior in which animals migrate away from their geographic area of origin and then return to reproduce in the same location where they began life. Although diverse long-distance migrants accomplish natal homing, little is known about how they do so. The enigma is epitomized by loggerhead sea turtles (*Caretta caretta*), which leave their home beaches as hatchlings and migrate across entire ocean basins before returning to nest in the same coastal area where they originated. One hypothesis is that turtles imprint on the unique geomagnetic signature of their natal area and use this information to return. Because Earth's field changes over time, geomagnetic imprinting should cause turtles to change their nesting locations as magnetic signatures drift slightly along coastlines (Fig. 17). To investigate, we analyzed a 19-year database of loggerhead nesting in the largest sea turtle rookery in North America.

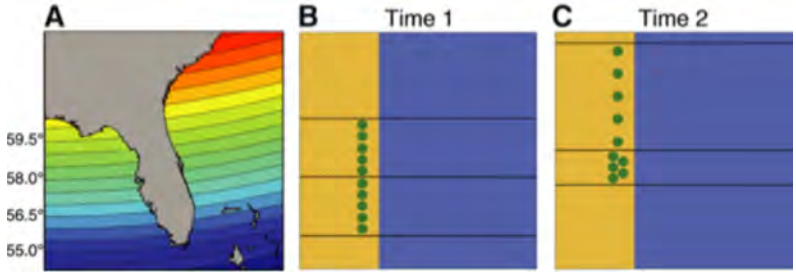

Fig. 17. Map showing magnetic inclination isolines near Florida and diagrams showing predicted effects of isoline movement on nesting density. (A) Because these isolines trend east/west whereas the coastline trends north/south, a unique magnetic inclination angle marks each area along Florida's east coast. Thus, turtles might locate natal beaches by returning to the appropriate isolines; locations to the north of the target area have steeper inclination angles, whereas locations to the south have shallower inclination angles. Black isolines bordering each color indicate increments of 0.5 degrees and were derived from the IGRF model 11 for the year 2012. The map for intensity isolines is not shown but is qualitatively similar, with different isolines of intensity existing at each area along Florida's east coast. (B and C) Horizontal lines indicate three hypothetical isolines, and green dots represent nesting turtles, each of which has imprinted on the magnetic signature that marked her natal site as a hatchling. Over the past two decades, isolines near Florida have moved northward, but at variable rates. Sometimes, isolines to the south moved less than those to the north, resulting in divergence (C; upper two isolines). In these situations, the geomagnetic imprinting hypothesis predicts a decrease in nesting density, because turtles that imprinted on the fields between the isolines should return to nest over a larger area. In places where isolines converged (because those to the south moved more than those to the north), the hypothesis predicts that nesting density should increase (C; lower two isolines). Tan represents land; blue represents sea.

We found a strong association between the spatial distribution of turtle nests and subtle changes in Earth's magnetic field. Nesting density increased significantly in coastal areas where magnetic signatures of adjacent beach locations converged over time, whereas nesting density decreased in places where magnetic signatures diverged (Fig. 18). These findings provide strong evidence that imprinting on magnetic inclination angle, magnetic intensity, or both plays an important role in the natal homing in sea turtles.

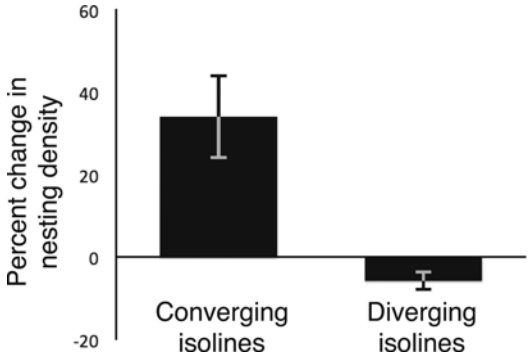

Fig. 18. Changes in nesting density for coastal areas with converging and diverging inclination isolines. At times and places in which isolines converged (n = 29), nesting density increased by an average of 35%. At times and places in which isolines diverged (n = 172), nesting density decreased by an average of 6%. The mean changes of the two groups were significantly different ($p = 5.34 \times 10^{-4}$). Error bars represent standard error of the mean. Figure is from Brothers and Lohmann (2015). Additional figures and a more detailed data analysis are included in this published paper.

Magnetic Navigation and Genetic Differences Among Sea Turtle Nesting Populations

Sea turtles are famous for natal homing, a pattern of behavior in which animals leave their area of origin when young, migrate long distances away, and eventually return as adults to reproduce in the same areas where they began life. Growing evidence suggests that sea turtles imprint on the magnetic field of their home beach soon after hatching and use this information to navigate back as adults, but magnetic navigation is difficult to study in large adult sea turtles, which often weigh in excess of 100 kg (220 lbs). As a novel way to gain insight into the mechanisms used by adult turtles to navigate to their natal beaches, we investigated the population structure of loggerhead sea turtles that nest in Florida.

The genetic structure of loggerhead sea turtles in Florida is unusual because populations of turtles that nest on east Florida beaches often are genetically different from other populations that nest a short distance away. At the same time, populations that nest on the east coast of Florida are often genetically similar to populations that nest on the west coast of Florida at about the same latitude. This pattern cannot be explained by the normal concept of "isolation by distance", which predicts that neighboring populations will be genetically similar and geographically distant populations will be genetically distinct. However, it might be explained if turtles return to their natal beaches by seeking out a particular magnetic field, because the fields that exist at similar latitudes on opposite sides of Florida are similar.

An analysis of loggerhead turtle population structure in the southeastern U.S. revealed that spatial variation in Earth's magnetic field does indeed strongly predict genetic differentiation between nesting areas, while geographic distance does not (Brothers and Lohmann, 2018; Fig. 19). These findings provide strong evidence that turtles use magnetic information to navigate

back to their natal beaches, and also imply that magnetic navigation underlies sea turtle population structure, inasmuch as the extent to which two nesting populations differ genetically is correlated with the difference between the magnetic fields that exist in the locations where the two groups nest. The methods developed for this analysis represent an important advance because they provide a potential way to investigate the navigational mechanisms used by animals that display natal homing, even if the animal in question is too large to be studied experimentally (e.g. elephant seals, whales, sharks, etc.).

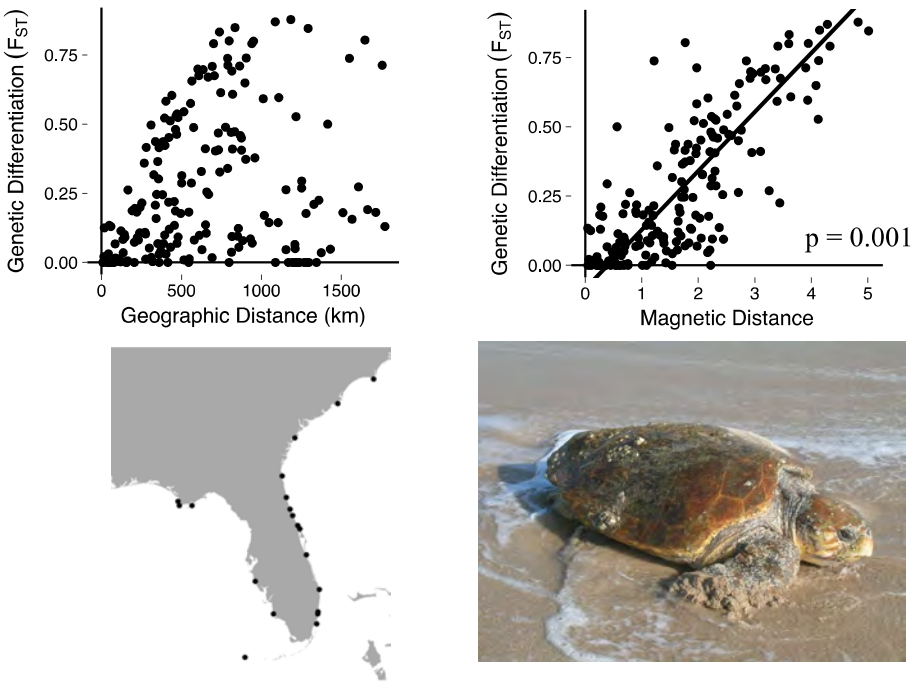

Fig. 19. Top: Regression analyses showing the relationship between F_{ST} and the geographic distance (top left) and between FST and the magnetic distance (top right). F_{ST} is a widely used metric of genetic differentiation that ranges from zero to one, with low values indicating genetic similarity and high values indicating genetic differentiation. In the regression plots, each data point represents a pairwise comparison between two nesting beaches with the genetic differentiation between nesting beaches on the y axis and geographic or magnetic distance between the nesting beaches on the x axis. Top left: No significant relationship was observed between genetic differentiation and geographic distance. Top right: A strong positive relationship exists between magnetic distance and genetic differentiation ($p = 0.001$); nesting beaches with similar magnetic fields harbor populations of turtles that are genetically similar, while nesting beaches with different magnetic fields are home to populations of turtles that are genetically. Bottom left: map showing locations (black dots) where the genetics of populations of nesting loggerhead turtles has been studied in the past (the genetic data we used was drawn from previously published studies). Bottom right: An adult loggerhead sea turtle returning to the ocean after digging her nest and laying eggs. The regression plots and map are from Brothers and Lohmann (2018).

Multi-modal navigation in sea turtles

Sea turtles are capable of navigating across large expanses of ocean to arrive at remote islands for nesting, but how they do so has remained enigmatic. An interesting example involves

green turtles (*Chelonia mydas*) that nest on Ascension Island, a tiny land mass located approximately 2000 km from the turtles' foraging grounds along the coast of Brazil. Sensory cues that turtles are known to detect, and which might hypothetically be used to help locate Ascension Island, include Earth's magnetic field, airborne odorants, and waterborne odorants. One possibility is that turtles use magnetic cues to arrive in the vicinity of the island, then use chemical cues to pinpoint its location. As a first step toward investigating this hypothesis, we used oceanic, atmospheric, and geomagnetic models to assess whether magnetic and chemical cues might plausibly be used by turtles to locate Ascension Island. Results suggest that waterborne and airborne odorants alone are insufficient to guide turtles from Brazil to Ascension, but might permit localization of the island once turtles arrive in its vicinity. By contrast, magnetic cues might lead turtles into the vicinity of the island, but would not typically permit its localization because the field shifts gradually over time. Simulations reveal, however, that the sequential use of magnetic and chemical cues can potentially provide a robust navigational strategy for locating Ascension Island (Endres et al., 2016). Specifically, one strategy that appears viable is following a magnetic isoline into the vicinity of Ascension Island until an odor plume emanating from the island is encountered, after which turtles might either: (1) initiate a search strategy; or (2) follow the plume to its island source. Details of this analysis have been published (Endres et al., 2016). These findings are consistent with the hypothesis that sea turtles, and perhaps other marine animals, use a multi-modal navigational strategy for locating remote islands.

Distributed Sensing of Magnetic Field Intensity in Biology and Engineering

In addition to detecting the direction of Earth's magnetic field, sea turtles also detect its strength or intensity. How they do so, however, is not known. One hypothesis is that multiple sensors that encode direction are simultaneously used to encode intensity, because the variance in direction encoded by the sensor population should decrease with increasing field strength. Working in collaboration with Dr. Brian Taylor, a visiting scientist from the Air Force Research Lab, we used the computational neuroscience tool of dynamic neural fields to investigate this conceptual model through simulations. In addition, we tested the performance of hardware consisting of an array of compasses constructed in accordance with the conceptual model. Results support the interpretation that the model provides a valid approach to encoding magnetic field information. Specifically, a population of magnetoreceptors, each of which is primarily devoted to detecting field direction, can collectively encode field intensity. This approach holds promise both as a possible biological solution for sensing magnetic field intensity, and also as an inspiration for sensing and processing paradigms in engineering. Details of this study have now been published (Taylor et al., 2017).

Behavioral Effects of Pulse-magnetization in Lobsters

The Caribbean spiny lobster is a migratory crustacean that uses Earth's magnetic field as a navigational cue, but how lobsters detect magnetic fields is not known. Magnetic material thought to be magnetite has previously been detected in spiny lobsters, but its role in magnetoreception, if any, remains unclear. As a first step toward investigating whether lobsters might have magnetite-based magnetoreceptors, we subjected lobsters to strong, pulsed magnetic fields capable of reversing the magnetic dipole moment of biogenic magnetite crystals. Groups of lobsters were subjected to a single pulse directed from posterior to anterior and either: (1) parallel to the horizontal component of the geomagnetic field (i.e., toward magnetic north); or (2)

antiparallel to the horizontal field (i.e., toward magnetic south). An additional control group was handled but not subjected to a magnetic pulse. After treatment, each lobster was tethered in a water-filled arena located within 200 m of the capture location and allowed to walk in any direction. Control lobsters walked in seemingly random directions and were not significantly oriented as a group. In contrast, the two groups exposed to pulsed fields were significantly oriented in approximately opposite directions (Fig. 20). Lobsters subjected to a magnetic pulse applied parallel to the geomagnetic horizontal component walked westward; those subjected to a pulse directed antiparallel to the geomagnetic horizontal component oriented approximately northeast. The finding that a magnetic pulse alters subsequent orientation behavior is consistent with the hypothesis that magnetoreception in spiny lobsters is based at least partly on magnetite-based magnetoreceptors. A paper describing these results has been published (Ernst and Lohmann, 2016).

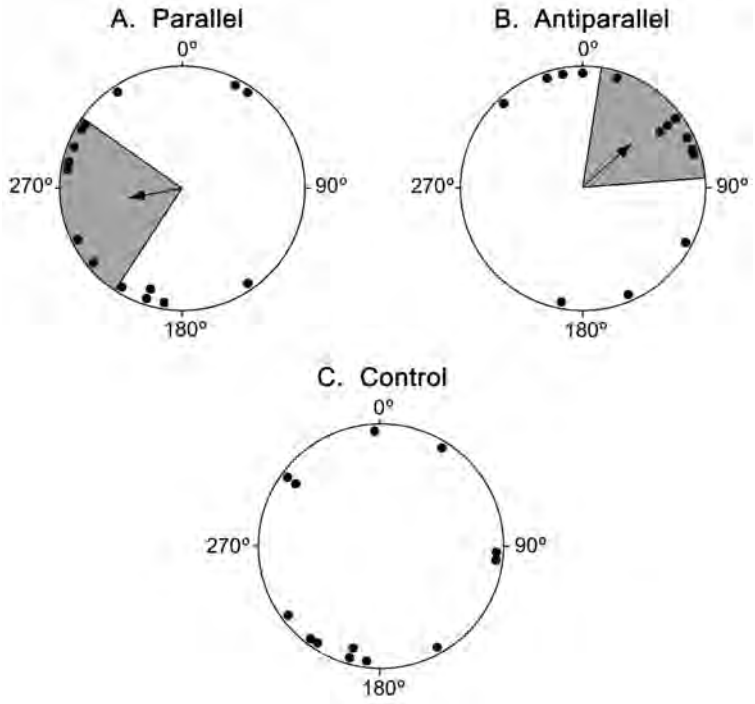

Fig. 20. Results of lobster pulse-magnetization experiment. (A) lobsters treated with a pulse directed parallel to the geomagnetic field horizontal field were significantly oriented with a mean angle of 259 deg. (B) Lobsters treated with a pulse directed antiparallel to the geomagnetic field horizontal component were significantly oriented in approximately the opposite direction, with a mean angle of 47 deg. (C) Control lobsters were not oriented as a group. Each black circle represents the mean heading of an individual lobster. Arrows indicate the mean direction of the group. Shaded areas represent the 95% confidence interval for the mean.

Behavioral Effects of Pulse Magnetization in Pacific Salmon

Among teleost fish, growing evidence suggests that crystals of the mineral magnetite provide the physical basis of the magnetic sense. As a first step toward investigating this hypothesis, juvenile Chinook salmon (*Oncorhynchus tshawytscha*) were exposed to a brief but strong magnetic pulse capable of altering the magnetic dipole moment of biogenic magnetite. Orientation behavior of pulsed fish and untreated control fish was then compared in a magnetic coil system under two conditions: (1) the local magnetic field; and (2) a magnetic field that exists near the southern boundary of the natural oceanic range of Chinook salmon.

Under local magnetic field conditions, fish from the control treatment group were significantly oriented with a mean angle of 338 degrees (Fig. 21A). In contrast, fish from the pulse group exhibited orientation that was statistically indistinguishable from random (Fig. 21B). No significant difference between the orientation of the control and pulse group was observed in the local field. When exposed to a magnetic field that exists near the southern limit of the Chinook salmon range, control fish had orientation that was statistically indistinguishable from random (Fig. 21C). In contrast, pulsed fish were significantly oriented towards the east-northeast with a mean angle of 72 degrees (Fig. 21D). The orientation of control and pulsed fish differed significantly.

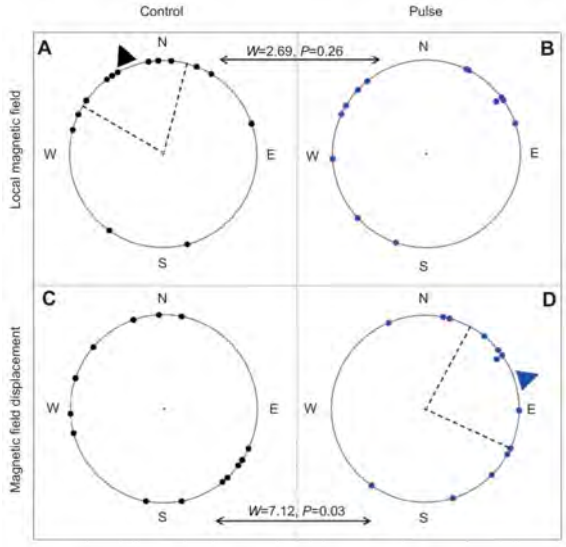

Fig. 21. Orientation of salmon under two different magnetic fields. (A) In the local magnetic field, fish from the control group were significantly oriented with a mean angle of 338 deg (Rayleigh test, n=14, r=0.55, P=0.01). (B) In the local magnetic field, salmon that experienced a strong magnetic pulse were not oriented as a group (Rayleigh test, n=13, r=0.37, P=0.18). (C) During a magnetic displacement to a southern ocean region, control fish were not oriented as a group (Rayleigh test, n=14, r=0.13, P=0.81). (D) During the magnetic displacement, salmon from the pulse group were significantly oriented with a mean angle of 72 deg (Rayleigh test, n=13, r=0.51, P=0.03). Each data point represents the mean angle of 16 fish that were tested in the coil simultaneously. Arrowheads indicate the mean direction of each treatment group. Dashed lines represent the 95% confidence intervals for the mean.

The results demonstrate that a strong magnetic pulse influences the subsequent orientation behavior of juvenile Chinook salmon. Salmon from the pulse and control groups exhibited significantly different orientation when tested in a magnetic field that exists near the southern boundary of their oceanic range (Fig. 21C,D). These results are the first to demonstrate that a magnetic pulse affects orientation behavior in fish. The findings are consistent with the magnetite hypothesis of magnetoreception, inasmuch as a magnetic pulse can potentially alter magnetite-based receptors, but should not exert any lasting effect on either chemical magnetoreception or electromagnetic induction. A full report on these findings has now been published (Naisbett-Jones et al., 2020).

Avoidance of Magnetic Gradients by Lobsters

On a global scale, the geomagnetic field varies predictably across Earth's surface, providing animals that migrate long distances with a reliable source of directional and positional information that can be used to guide their movements. In some locations, however, magnetic minerals in Earth's crust generate an additional field that enhances or diminishes the overall field, resulting in unusually steep gradients of field intensity within a limited area. How animals respond to such magnetic anomalies is unclear.

As a first step toward investigating whether magnetic anomalies affect the behavior of lobsters, a two-choice preference experiment (Ernst and Lohmann, 2018) was conducted in which lobsters were allowed to select one of two artificial dens, one beneath a neodymium

magnet and the other beneath a non-magnetic weight of similar size and mass (control). Significantly more lobsters selected the control den, demonstrating avoidance of the magnetic anomaly. The results suggest the possibility that lobsters avoid magnetic anomalies that might otherwise interfere with successful magnetic navigation. In addition, the findings are consistent with magnetite-based magnetoreception, inasmuch as a strong magnetic gradient exerts a force on magnetic crystals; one possible interpretation is therefore that lobsters approaching magnets experience unusual or unpleasant sensations arising from secondary receptors that transduce the movement of magnetite crystals to the nervous system.

Development of Behavioral Assay for Magnetic Map Responses in Sea Turtles

One long-term challenge in magnetoreception research has been to develop behavioral assays that can be used to distinguish between a magnetic directional sense (or "compass") and a magnetic positional sense (or "map"). This is important because of the possibility that different mechanisms may underlie the compass and map. For example, some birds have been hypothesized to have a compass based on cryptochromes and radical pair chemistry, but a map based on magnetite. In many experimental settings, it is impossible to study magnetic responses of animals and know with certainty whether an experimental manipulation is affecting a compass, a map, or both.

Sea turtles are unusual among magnetically sensitive animals in that they are known to have not only a magnetic compass that detects field direction, but also a magnetic map based on the predictable spatial variation of Earth's magnetic field. Due to this variation, different geographic locations have slightly different magnetic fields; thus, most foraging areas that turtles inhabit have unique "magnetic signatures". During the past two years, we have focused on developing a unique behavioral assay that can be used to investigate the basis for the sea turtle's magnetic map sense.

Juvenile sea turtles reliably return to specific foraging grounds following seasonal migrations and experimental displacements. In principle, this foraging site fidelity may be accomplished by turtles learning the magnetic signature of that site and then navigating back to it magnetically. To investigate this possibility, we tested whether turtles can learn to associate a specific magnetic signature with food.

For these experiments, captive loggerhead turtles (*Caretta caretta*) approximately three months of age were tested inside a large magnetic coil system that could be used to reproduce the magnetic field that exists at any location in the Atlantic Ocean. The turtles were assigned to one of two different experimental groups. Each group was exposed to two different magnetic fields (each from a different location in the Atlantic Ocean) on a daily alternating schedule. One magnetic field replicated a field at a location north of the turtles' home (North Carolina), and the other replicated a field south of the turtles' home. Importantly, the turtles had never been to either location in nature. On days when the turtles were exposed to the north field, the north group received food. On days when the turtles were exposed to the south field, the south group received food. Thus, each group was exposed to the same two magnetic fields repeatedly but conditioned to only one of them.

Captive turtles rapidly acquire 'food-seeking behavior' under conditions in which they expect to be fed. This behavior consists of swimming at the surface with the head out of the water and the mouth open, apparently in anticipation of food being dropped into the tank. In post-conditioning trials conducted in the absence of food, turtles were exposed to both fields. Turtles in each group exhibited higher levels of food-seeking behavior when exposed to the

magnetic field in which they had previously been fed (Fig. 22). Turtles have now been conditioned to associate food with four different natural magnetic fields that exist in geographic locations between Canada and Cuba. These findings demonstrate that turtles are able to learn diverse magnetic fields that exist over a large geographic area, as would be expected if they are able to learn the fields associated with food-rich locations.

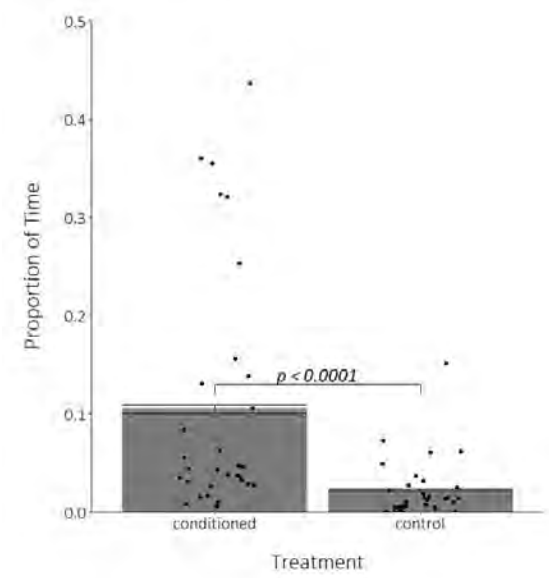

Fig. 22. Time spent exhibiting food-seeking behavior for turtles (n=32) tested under two magnetic field conditions. "Conditioned" indicates tests in a magnetic field in which the turtle had previously been fed for 60 days. "Control" indicates tests in a magnetic field in which the turtle was never previously fed. During tests, no food was present. Each black dot represents one individual turtle's response. Error bars represent standard error. Turtles spent significantly more time exhibiting food-seeking behavior when tested in a field in which they had previously been fed, demonstrating that they can distinguish among "magnetic signatures" of different locations.

These results provide the first direct evidence that sea turtles can learn to associate a magnetic field with food, a process that may underlie the development of foraging site fidelity. In the context of our research program, the finding is an important advance because it provides the first behavioral assay that is dependent entirely upon magnetic positional (or magnetic map) information. Thus, this assay can serve as a foundation for future tests in which stimuli are introduced that might disrupt one of the hypothesized mechanisms of magnetoreception.

Evidence for Magnetic Navigation in Whales

Relatively little is known about how large marine mammals, such as whales, accomplish their impressive long-distance migrations, and whether magnetic navigation is involved. Baleen whales are an ideal candidate group for investigating magnetoreception in mammals due to their long migrations and the unique navigational challenges they face in the featureless open ocean. In this environment, it might be advantageous to derive navigational cues from the relatively constant and ubiquitous geomagnetic field. While it is difficult to perform behavioral experiments on whales, it might be possible to use live stranding data (strandings in which the whale may have made a navigational error, rather than those in which a whale died at sea and washed ashore) as a tool for investigating their navigational senses.

Some live strandings of whales are thought to result from navigational errors because some stranded individuals exhibit no signs of illness or injury and resume normal activity when returned to the sea. Thus, whale stranding data may act as a proxy for a disturbed navigational system. We hypothesized that magnetoreceptive whales would strand more often on days with increased magnetic noise. To test this hypothesis, we acquired U.S. migrating gray whale (*Eschrichtius robustus*) stranding data spanning 1985-2018 (n=186) and showed that there is a 2.1-fold increase in the likelihood of a live gray whale stranding on days with a high sunspot

count than on low sunspot days. Increased sunspot count is strongly correlated with solar storms – sudden releases of high-energy particles from the sun that cause extreme disruptions to human communication and navigation technology. To further explore this relationship, we looked at several variables measured on the earth which are affected by solar storms and found a 3.7-fold increase in the likelihood of a live stranding on days with high radio frequency (RF) noise, but no effect when relative to horizontal displacements in the earth's magnetic field as measured by the Ap index. This work suggests that the mechanism for the relationship between high sunspot number and live strandings may be a disruption of the magnetic sense, rather than distortion of the geomagnetic field itself. RF noise has been shown to disrupt magnetic orientation in certain species. A full account of this work has now been published (Granger et al., 2020).

Bio-inspired Magnetic Navigational Strategies

The magnetic navigation strategies of animals provide a possible source of inspiration for the design of engineered systems. In a collaborative project with Dr. Brian Taylor, we have investigated how animals might, in principle, use magnetic inclination (i.e., the angle between the magnetic field vector and the surface of the earth) as a means of global navigation. In simulations, an artificial agent was tasked with executing a series of trans-equatorial migrations using sequential measurements of magnetic inclination. The agent was tested both in a magnetic field resembling that of the present geomagnetic field and in a field with reversed polarity. The findings: (1) demonstrate that using sequential inclination measurements is a feasible way to execute a trans-equatorial migration; and (2) suggest that an inclination-based navigation strategy is tolerant of field reversals. The results have provided insight into how both animals and autonomous vehicles might navigate using magnetic inclination, particularly as the magnetic field changes over time. The results may be useful in the development of new autonomous engineered navigation systems. A paper describing these results (Taylor et al., in press) has been accepted for publication in the *Journal of the Royal Society Interface*.

Publications during full period of grant

Arniella, M.B., Fitak, R.R., and S. Johnsen. 2018. Unmapped sequencing reads identify additional candidate genes linked to magnetoreception in rainbow trout. *Environmental Biology of Fishes.* 101(5): 711-721.

Barrick, J., Doblas, A., Gardner, M.R., Sears, P.R., Ostrowski, L.E., and A.L. Oldenburg. 2016. High-speed and high-sensitivity parallel spectral-domain optical coherence tomography using a supercontinuum light source. *Optics Letters* 41(24): 5620-5623.

Brothers, J.R. and K.J. Lohmann. 2015. Evidence for geomagnetic imprinting and magnetic navigation in the natal homing of sea turtles. *Current Biology* 25: 392-396.

Brothers, J.R. and K.J. Lohmann. 2018. Evidence that magnetic navigation and geomagnetic imprinting shape spatial genetic variation in sea turtles. *Current Biology* 28: 1325-1329.

Endres, C.S., Putman, N.F., Ernst, D.A., Kurth, J.A., Lohmann, C.M.F. and K.J. Lohmann. 2016. Multi-modal homing in sea turtles: modeling dual use of geomagnetic and chemical cues in island-finding. *Frontiers in Behavioral Neuroscience* 10.

Ernst, D.A., Fitak, R.R., Schmidt, M., Derby, C.D., Johnsen, S., and K.J. Lohmann. 2020. Pulse magnetization elicits differential gene expression in the central nervous system of the Caribbean lobster, *Panulirus argus*. *Journal of Comparative Physiology A* 206, 725-742.

Ernst, D.A. and K.J. Lohmann. 2016. Effect of magnetic pulses on Caribbean spiny lobsters: implications for magnetoreception. *Journal of Experimental Biology* 219: 1827-1832. doi:10.1242/jeb.136036

Ernst, D.A. and K.J. Lohmann. 2018. Size-dependent avoidance of a strong magnetic anomaly in Caribbean spiny lobsters. *Journal of Experimental Biology* 221, jeb172205.

Fitak, R.R. and S. Johnsen. 2017. Bringing the statistical analysis of animal orientation full circle: model-based approaches with maximum likelihood. *Journal of Experimental Biology* 220: 3878-38882.

Fitak RR and S. Johnsen. 2018. Green sea turtle (*Chelonia mydas*) population history indicates important demographic changes near the mid-Pleistocene transition. *Marine Biology* 165(7): 110.

Fitak, R.R., Schweikert, L.E., Wheeler, B.R., Ernst, D.A., Lohmann, K.J., and S. Johnsen. 2018. Near absence of differential gene expression in the retina of rainbow trout after exposure to a magnetic pulse: implications for magnetoreception. *Biology Letters* 14: 20180209 http://dx.doi.org/10.1098/rsbl.2018.0209

Fitak, R.R., Wheeler, B.R., Ernst, D.A., Lohmann, K.J., and S. Johnsen. 2017. Candidate genes mediating magnetoreception in rainbow trout (*Oncorhynchus mykiss*). *Biology Letters* 13(4): 20170142.

Fitak R.R., Wheeler B.R. and S. Johnsen. 2020. Effect of a magnetic pulse on orientation behavior in rainbow trout (*Oncorhynchus mykiss*). *Behavioral Processes* 172: 104058.

Granger, J., Walkowicz, L., Fitak, R.R. and S. Johnsen. 2020. Gray whales strand more often on days with increased levels of atmospheric radio-frequency noise. *Current Biology* 30: R155-R156.

Hossein, M., Levy, B.E., Thapa, D., Oldenburg, A.L. and C.M. Gallippi. 2018. Blind source separation based motion detector for imaging super-paramagnetic iron oxide (SPIO) particles in magnetomotive ultrasound imaging. *IEEE Transactions on Medical Imaging* doi:10.1109/TMI.2018.2848204.

Johnsen, S., Lohmann, K.J., and E. Warrant. 2020. Animal navigation: a noisy magnetic compass? *Journal of Experimental Biology*. 223, jeb164921. doi:10.1242/jeb.164921.

Lavine, M., Brothers, J.R., Lohmann, K.J. and I. Lavine. 2016. Sea turtles: A case of animal magnetism. *Chance* 29 (2): 4-9.

Levy, B.E., Hossain, M.M., Gallippi, C.M. and A.L. Oldenburg. 2018. Effect of model thrombus volume and elastic modulus on magnetomotive ultrasound signal under pulsatile flow. *IEEE Transactions on Ultrasonics, Ferroelectrics, and Frequency Control* (TUFFC). doi:10.1109/TUFFC.2018.2841774.

Lohmann, K.J. 2018. Animal migration research takes wing. *Current Biology* 28, R952-R955 (invited commentary).

Lohmann, K.J. and C.M.F. Lohmann. 2019. There and back again: natal homing by magnetic navigation in sea turtles and salmon. *Journal of Experimental Biology*, *222*, jeb184077.

Naisbett-Jones, L.C., Putman, N.F., Scanlan, M.M., Noakes, D.L. and K.J. Lohmann. 2020. Magnetoreception in fishes: the effect of magnetic pulses on orientation of juvenile Pacific salmon. *Journal of Experimental Biology* 223(10).

Taylor, B.K., Johnsen, S., and K.J. Lohmann. 2017. Detection of magnetic field properties using distributed sensing: a computational neuroscience approach. *Bioinspiration and Biomimetics* 12(3): 036013.

Taylor, B.K., Lohmann, K.J., Havens, L.T., Lohmann, C.M.F., and J. Granger. In press. Long-distance transequatorial navigation using sequential measurements of magnetic inclination angle. *Journal of the Royal Society Interface.*

Thapa, D., Levy, B., Marks, D. L., and A. L. Oldenburg. 2019. Inversion of displacement fields to quantify the magnetic particle distribution in homogeneous elastic media from magnetomotive ultrasound. *Physics in Medicine and Biology*. 64(12): 125019.

Paper in preparation

J. Barrick and A. L. Oldenburg. “Single magnetic particle detection with line-field magneto-motive optical coherence tomography.” In preparation for submission to *Optics Letters*.

Ph.D. Dissertations supported by the grant

Barrick, J. 2020. Development of a line-field magneto-motive optical coherence tomography system. *Doctoral dissertation, Physics Department, University of North Carolina at Chapel Hill*.

Brothers, J. R. 2018. Population level and behavioral investigations of geomagnetic imprinting and natal homing in sea turtles. *Doctoral dissertation, Biology Department, University of North Carolina at Chapel Hill*.

Ernst, D.A. 2018. Magnetoreception and its neural basis in spiny lobsters. *Doctoral dissertation, Biology Department, University of North Carolina at Chapel Hill*.